ISTANBUL TECHNICAL UNIVERSITY ★ GRADUATE SCHOOL

ENERGY DISSIPATION AND RATE-DEPENDENT DEFORMATION BEHAVIOR OF STF-INTEGRATED PU FOAM NANOCOMPOSITES

M.Sc. THESIS

Emre GÜNDÜZ

Department of Polymer Science and Technology

Polymer Science and Technology Programme

JUNE 2023

ISTANBUL TECHNICAL UNIVERSITY ★ GRADUATE SCHOOL

ENERGY DISSIPATION AND RATE-DEPENDENT DEFORMATION BEHAVIOR OF STF-INTEGRATED PU FOAM NANOCOMPOSITES

M.Sc. THESIS

Emre GÜNDÜZ
(515191022)

Department of Polymer Science and Technology

Polymer Science and Technology Programme

Thesis Advisor: Assoc. Prof. Bünyamin KARAGÖZ

JUNE 2023

İSTANBUL TEKNİK ÜNİVERSİTESİ ★ LİSANSÜSTÜ EĞİTİM ENSTİTÜSÜ

STF ENTEGRE PU KÖPÜK NANOKOMPOZİTLERİN ENERJİ EMME VE HIZA BAĞLI DEFORMASYON DAVRANIŞI

YÜKSEK LİSANS TEZİ

Emre GÜNDÜZ
(515191022)

Polimer Bilimi ve Teknolojisi Anabilim Dalı

Polimer Bilimi ve Teknolojisi Programı

Tez Danışmanı: Doç. Dr. Bünyamin KARAGÖZ

HAZİRAN 2023

Emre GÜNDÜZ, a M.Sc. student of ITU Graduate School of student ID 515191022, successfully defended the thesis entitled "ENERGY DISSIPATION AND RATE-DEPENDENT DEFORMATION BEHAVIOR OF STF-INTEGRATED PU FOAM NANOCOMPOSITES", which he prepared after fulfilling the requirements specified in the associated legislations before the jury whose signatures are below.

Thesis Advisor:	**Assoc. Prof. Bünyamin KARAGÖZ** Istanbul Technical University	……..
Jury Members:	**Assoc. Prof. Hülya CEBECİ** Istanbul Technical University	……..
	Prof. Dr. Aydan DAĞ Bezmialem Vakif University	……..

Date of Submission : 25 May 2023
Date of Defense : 08 June 2023

To my beloved family,

FOREWORD

First of all, I am thankful to my thesis advisor Assoc. Prof. Bünyamin Karagöz, and Assoc. Prof. Hülya Cebeci, Asst. Prof. Kaan YILDIZ and Dr. İpek ÖSKEN for accepting me to their research laboratories, for valuable insights, and directions giving me needful guidance to complete this thesis. Thanks to their kindness, patience, and supervision, I have my chance to improve myself in polymer synthesis, mechanical testing, rheological and morphological characterizations, and more. The contributions of the last three years beyond the technical knowledge, management skills, critical thinking, and presentation, trainings are indisputable, irreplaceable, and precious for me. I sincerely thank Dr. İpek ÖSKEN for not only her supervision but also her great attitude. I have enjoyed our conversations and discussions on all topics. I would like to thank TUBITAK (The Scientific and Technological Research Institution of Turkey) (Project number: 121M993) for supporting our project financially and funding the Material Research Society (MRS) FALL Meeting and Exhibit in Boston, MA, USA. I believe that attending this meeting provide me with a great experience and global vision.

I would also like to thank, ITU Aerospace Research Center (ARC) - Nanomaterials, Textiles and Advanced Composites Research Group, for opening their laboratory to complete my works with great pleasure during the course of the thesis. I will be in great depth for Melisa DİNÇER, Dilan ARSLAN, and Serkan ŞENEL for their understanding, motivation, and friendship, and also Merve KARABAL and Suat EBİL for their help in the thesis.

I am deeply grateful to my colleague, I met during the interview of this M.Sc., İlayda KORAMAZ for her patience, kindness, friendship. Her sense of humor made my academic life to enjoy it fully. She is the best "carlos" I have ever met. I would also like to take this opportunity also thank another "carlos" Bleda Can SADIKOĞULLARI for his help. As we always said "our intention is not to offend anyone". I would also like to thank Rabia BOZBAY, Sinem YILDIZ, and Özge AKÇA ZENGİN for their accompany and friendship.

My last thanks to my beloved family. İnci GÜNDÜZ, Cafer GÜNDÜZ, Selim GÜNDÜZ, Yağmur GÜNDÜZ, for always being on my side. Being born into a family like yours has been my greatest fortune, and the freedom and vision you provided me with have been invaluable. Honesty, confidence, and countless other virtues are things I have learned from you, and I can only learn from you.

Lastly, with the happiness and honor of having completed my master's thesis, I would like to express my gratitude to Mustafa Kemal Atatürk. I respectfully and gratefully remember him for his great efforts to modernize our country. I would like to end my words with a quote from him: "If one day my words are against science, choose science."

June 2023 Emre Gündüz

TABLE OF CONTENTS

Page

ABBREVIATIONS

ASTM	: American Standard Test Method
CNT	: Carbon Nanotube
DMA	: Dynamic Mechanical Analysis
EG	: Ethylene glycol
GO	: Graphene oxide
PEG	: Polyethylene glycol
PMDI	: Polymeric Diphenylmethane Diisocyanate
PU	: Polyurethane
Rpm	: Revolutions per minute
SEM	: Scanning Electron Microscopy
Std	: Standard Deviation
STF	: Shear Thickening Fluid
t/l	: Thickness to length ratio
UTM	: Universal Testing Machine
wt.%	: weight percentage

SYMBOLS

°C	: Celsius Degree
cm^3	: Cubic centimeter
g	: Gram
J	: Joule
m^3	: Cubic meter
MPa	: Mega Pascal
Pa	: Pascal
kg	: Kilogram
s	: Second
$\dot{\gamma}$	: Shear rate
η	: Loss factor
η_{max}	: Maximum viscosity
η_{min}	: Minimum viscosity
µm	: Micrometer
nm	: Nanometer

LIST OF TABLES

Page

LIST OF FIGURES

Page

ENERGY DISSIPATION AND RATE-DEPENDENT DEFORMATION BEHAVIOR OF STF-INTEGRATED PU FOAM NANOCOMPOSITES

SUMMARY

Designing energy absorptive structures is crucial for safety and these structures withstand several loads such as compression, bending, and impact. Beside to honeycombs as a core material for sandwich structures, polymeric foams receive great attention as structural components with their outstanding effective stress transfer, viscoelastic properties, and increased surface area. Among several polymeric foams, rigid polyurethane (PU) foams are good candidates presenting high strength and lightweight characteristics and tailorability. PU is a particular polymer group that stands out with its unique chemistry, typically synthesized from polyol and isocyanate, which also has a potential to fill the vacancies between rubbers and plastics based on their mechanical thermal and viscoelastic properties. PU foams can have densities that range from 20 to 3000 kg/m^3 which provide a wide range of application areas and properties. The physical and mechanical properties of PU foams are closely correlated to their morphological characteristics, which are mainly determined by several key parameters such as foam density, cell density, cell edge length, wall thickness, and thickness to length ratio (t/l). PU foams could be customized by incorporating nano and/or micro-sized reinforcing agents to obtain unique functionality and properties. Combining nanoparticle inclusion with process parameter optimization can result in improved mechanical properties and multifunctionality. Nanoparticles can act as nucleation points and lead to narrow cell edge length, increased cell wall thickness, and higher cell density, yielding advanced mechanical properties. Despite the considerable research into carbon-based nanostructures such as carbon nanotubes (CNTs) and graphene as reinforcing agents in polymeric foams to maximize their energy absorption capabilities and strength, further efforts are required to investigate the potential role of other nanomaterials, such as shear thickening fluids (STFs), which exhibit extraordinary energy absorption properties. STFs as colloid suspensions, at elevated shear rates, form hydroclusters due to particle interaction yielding a drastic viscosity increase. Thus, rapid viscosity change results in an excellent energy absorption characteristic. This study is aimed to improve the compressive and energy absorption properties of PU foams with STF integration while discussing the microstructure/mechanical property relationship. Initially, STFs were fabricated with up to 30 wt.% fumed and spherical silica content, using a mechanical stirrer at 300 rpm and horn sonicator with 30% amplitude, then investigated by a plate rheometer in order to understand the effect of particle geometry and weight fraction on the flow characteristics. The results revealed that 26 wt.% of fumed silica was the optimum suspension for integration to PU foam with the excellent thickening ratio, and viscosity values increased after critical shear rate up to 67.66 times. The 26 wt.% STFs were successfully integrated into rigid PU foams, using a mechanical stirrer prior to the foaming reaction, at 0.5, 1, and 3 wt.%, and the morphological analysis, compression, and cyclic compression tests at various strain rates up to 0.2 s^{-1} and 10, 40, 80% strains

in order to understand rate dependent properties under different deformation region such as plateau and densification, were performed. According to morphological characterizations, cell edge lengths decreased and cell wall thickness increased with increasing until 1 wt.% STF. The maximum t/l ratio, which is a favorable indicator for mechanical strength prediction, was observed with 1 wt.% STF integration into PU foam. The results showed that 1 wt.% STF presented the highest compressive strength and specific compressive strength with 33% and 10.4% increments, respectively. For the energy absorption properties, 1 wt.% STF demonstrated up to 9.4% higher loss factor and 46.9% total absorbed energy regarding cyclic compression tests strain and strain rate parameters. Dynamic mechanical analyses were also carried out, under bending loads with dual cantilever clamps, to develop the microstructure-mechanical property relationship and to examine the viscoelastic properties. Linear viscoelastic region and storage and loss moduli increased with 1 wt.% STF integration. The results were consistent with both the compression and cyclic compression tests, despite differences in the direction and frequency of the applied force. Integration of 1 wt.% STF resulted in a significant increase of approximately 50% in both storage and compression modulus, while no significant changes in loss factor were observed. By enhancing the storage modulus and broadening the linear elastic regime, STF/PU foams can effectively withstand higher levels of load and displacement without permanent deformation. Excessive STF integration, such as above 1 wt. %, caused deterioration in the foam morphology and cellular structure, resulting in lower mechanical properties and strengths, however the 3 wt.% STF integrated foam still exhibited better properties than neat foam. This study showed that the flow properties of STFs are significantly influenced by the silica surface geometry and weight fraction. Furthermore, the study demonstrated that the addition of an optimized amount of STF enhanced the compressive strength, viscoelastic properties, and energy absorption capabilities of PU foams. With the addition of STF, PU foams could be used in a wider range of application areas and their superior mechanical properties could be used to build safer and reliable structures.

STF ENTEGRE PU KÖPÜK NANOKOMPOZİTLERİN ENERJİ EMME VE HIZA BAĞLI DEFORMASYON DAVRANIŞI

ÖZET

Enerji emici yapıların tasarlanması emniyet ve güvenlik için oldukça önemlidir ve bu yapıların basma, eğilme ve darbe gibi çeşitli yüklere dayanması gerekmektedir. Sandviç yapılar için çekirdek (nüve) malzeme olarak bal peteklerinin yanı sıra, polimerik köpükler olağanüstü etkili yük transferi, viskoelastik özellikleri ve artan yüzey alanı ile yapısal bileşenler olarak büyük ilgi görmektedir. Çeşitli polimerik köpükler arasında, rijit poliüretan (PU) köpükler, yüksek mukavemet ve hafiflik özellikleri ve uyarlanabilirlik özellikleriyle iyi bir seçenek olarak değerlendirilebilir. PU köpükler, tipik olarak poliol ve izosiyanattan sentezlenen, mekanik, termal ve viskoelastik özelliklere göre kauçuklar ve plastikler arasındaki boşlukları doldurma potansiyeline sahip, benzersiz kimyası ile öne çıkan özel bir polimer grubudur. PU köpükler, geniş bir uygulama alanı ve özellik yelpazesi sağlayan 20 ila 3000 kg/m^3 arasında değişen yoğunluk değerlerine sahip olabilir. PU köpüklerin fiziksel ve mekanik özellikleri, esas olarak köpüğün yoğunluğu, hücre yoğunluğu, hücre kenarı uzunluğu, duvar kalınlığı ve kalınlık/uzunluk oranı (t/l) gibi birkaç temel parametre tarafından belirlenen morfolojik özellikleriyle yakından ilişkilidir. PU köpükler, benzersiz işlevsellik ve özellikler elde etmek için nano ve/veya mikro boyutlu takviye maddeleri eklenerek geliştirilebilmektedir. PU köpüğe nano parçacık takviyesinin proses parametresi optimizasyonu ile birleştirilmesi, gelişmiş mekanik ve fonksiyonel özellikler kazandırmaktadır. Mekanik özelliklerdeki artış, köpüğün mikro yapısındaki değişiklikten kaynaklanmaktadır. Hücre oluşumunda nano parçacıklar çekirdeklenme noktaları olarak görev alarak kısa hücre kenar uzunluğuna, daha geniş hücre duvarı kalınlığına ve daha yüksek hücre yoğunluğuna yol açarak gelişmiş mekanik özellikler sağlayabilmektedir. Enerji emme kabiliyetleri gerilim-gerinim eğrilerinden hesaplanan histeresiz alan, kayıp faktörü ve enerji kayıp katsayısı gibi değerlerle ölçülebilir. Bu ölçümler, enerji emici malzemelerin kullanıldığı uygulamalarda oldukça önemlidir. Çünkü enerjiyi verimli bir şekilde dağıtma yeteneği, uygulanan kuvvetlerin yapılar ve bileşenler üzerindeki etkisini azaltmada kritik öneme sahiptir. Uygulanan kuvvetler sonucu oluşan enerji, hücrelerin elastik/plastik deformasyonu, sürtünme ve ısı olarak emilebilmektedir. Polimerik köpüklerin enerji emme kabiliyetlerini ve mukavemetlerini en üst düzeye çıkarmak için karbon nanotüpler ve grafen gibi karbon bazlı nano yapıların takviye edici maddeler olarak kullanılmasına yönelik önemli araştırmalar yapılmasına rağmen, olağanüstü enerji emme özellikleri sergileyen kesme altında katılaşan sıvılar (STF'ler) gibi diğer nano malzemelerin potansiyel rolünü araştırmak için daha fazla çaba sarf edilmesi gerekmektedir. STF'ler, sıvı ve katıların karışımından oluşan kolloid süspansiyonlar olup, yüksek kesme hızlarında, parçacık etkileşimleri nedeniyle hidrokümeler oluşturarak ciddi bir viskozite artışı sağlar. Böylece, hızlı viskozite değişimi mükemmel bir enerji absorbsiyonu özelliği ile sonuçlanır. PU köpükler üstün enerji emilimi ve ısı yalıtımı özelliklerine sahiptir, bu nedenle STF'lerin sert PU köpüğe entegrasyonu STF'lerin

akış davranışını stabilize edebilir, ayrıca STF sızıntılarını önleyebilir ve daha yüksek enerji emilimi sağlayan malzemeler elde edilebilir. Bu çalışma, mikroyapı / mekanik özellik ilişkisini tartışırken, PU köpüklerin basma ve enerji emme özelliklerini STF entegrasyonu ile geliştirmeyi amaçlamaktadır. Başlangıçta, STF'ler ağırlıkça %30'a kadar füme ve küresel silika içeriği ile 300 rpm'de mekanik karıştırıcı ve %30 genlikli çalışan horn sonikatör kullanılarak üretilmiş, daha sonra parçacık geometrisi ve ağırlık oranının STF'nin akış özellikleri üzerindeki etkisini anlamak amacıyla reometreyle incelenmiştir. Sonuçlar, ağırlıkça %26 füme silika içeren STF'in 67.66 değerinde mükemmel kalınlaşma oranıyla PU köpüğe entegrasyon için optimum süspansiyon olduğunu, kesme hızının artmasıyla birlikte viskozite değerlerinin 0.74 Pa.s'den 50.07 Pa.s'ye arttığını ortaya koymuştur. Ek olarak üretim gününden 32 gün sonrasına kadar belirli zaman aralıklarıyla yapılan reolojik ölçümler ışığında, akış özelliklerinin üretim gününden 1 aydan fazla zaman geçmesine rağmen ilk günkü özelliklerini sergilediği gözlemlenmiştir. Ağırlıkça %26 füme silika içeren STF, poliüretan (köpükleşme) sentezinden önce mekanik karıştırıcı kullanılarak köpüğün ağırlığına göre ağırlıkça %0,5, %1 ve %3 oranlarında poliol ortamında disperse edilmiş daha sonrasında köpükleşme reaksiyonuyla birlikte STF katkılı sert PU köpükler elde edilmiştir. Elastik, plato ve densifikasyon gibi farklı deformasyon bölgeleri altında orana bağlı özellikleri anlamak için optik mikroskop ve taramalı elektron mikroskopuyla morfolojik analiz, 0,2 s^{-1}'e kadar çeşitli gerinim hızlarında basma testleri ve %10, %40, %80 uygulanan gerinimlerde döngüsel basma testleri gerçekleştirilmiştir. Morfolojik incelemelere göre, ağırlıkça %1 STF takviyesine kadar hücre kenar uzunlukları azalmış ve hücre duvar kalınlığı artmıştır. Mekanik mukavemet tahmini için uygun bir gösterge olan t/l oranı, PU köpüğe ağırlıkça %1 STF entegrasyonuyla maksimum seviyeye ulaşmıştır. Basma testi sonuçlarının morfolojik incelemelerle uyumlu olduğu gözlemlenmiş STF katkısıyla birlikte artan t/l oranının yanı sıra basma dayanımının da arttığı görülmüştür. Sonuçlar ışığında, ağırlıkça %1 STF katkısının sırasıyla %33 ve %10,4'lük artışlarla en yüksek basma dayanımı ve özgül basma dayanımını sunduğunu göstermiştir. Densifikasyon bölgesinde hücrelerin kırılması sonucu gözlenen en yüksek gerilim değeri ağırlıkça %1 STF katkısıyla, katkılanmamış köpüğe göre %50'den fazla artmıştır. Enerji absorpsiyon özellikleri için, ağırlıkça %1 STF, döngüsel sıkıştırma testleri gerinim ve gerinim hızı parametrelerine göre %9,4'e kadar daha yüksek kayıp faktörü ve %46,9'a kadar daha fazla toplam absorbe edilen enerji göstermiştir. Mikroyapı-mekanik özellik ilişkisini geliştirmek ve viskoelastik özellikleri incelemek için eğilme yükü altında dinamik mekanik analiz testleri gerçekleştirilmiştir. Doğrusal viskoelastik bölge ile depolama ve kayıp modülleri ağırlıkça %1 STF entegrasyonu ile artmıştır. Sonuçlar, uygulanan kuvvetin yönü ve frekansındaki farklılıklara rağmen hem basma hem de döngüsel basma testleriyle tutarlı olduğu gözlemlenmiştir. Ağırlıkça %1 STF entegrasyonu hem enerji depolama hem de basma modülünde yaklaşık %50 civarında önemli bir artışa sebep olurken, kayıp faktöründe önemli bir değişiklik gözlenmemiştir. Depolama modülünü artırarak ve doğrusal elastik rejimi genişleterek, STF/PU köpükler kalıcı deformasyona uğramadan, daha şiddetli kuvvet ve uzun yer değiştirme seviyelerine etkili bir şekilde dayanım sağlayabilir. Ağırlıkça %1'in üzerindeki STF takviyeleri, köpük morfolojisinde ve hücresel yapıda bozulmaya neden olarak daha düşük mekanik özellikler ve mukavemetlerle sonuçlanmıştır, ancak ağırlıkça %3 STF katkılı köpük yine de katkısız köpükten daha yüksek basma dayanımı ve enerji absorbsiyonu sergilemiştir. Bu çalışma, STF'lerin akış özelliklerinin silika yüzey geometrisi ve ağırlık fraksiyonundan önemli ölçüde etkilendiğini göstermiştir. Ayrıca çalışma, optimize edilmiş miktarda STF ilavesinin PU köpüklerin basma dayanımını,

viskoelastik özelliklerini ve enerji emme kabiliyetlerini artırdığını göstermiştir. STF ilavesiyle, PU köpükler daha geniş bir uygulama alanında kullanılabilir ve üstün mekanik özellikleri sayesinde daha güvenli ve emniyetli yapılar inşa etmek için kullanılabilir.

1. INTRODUCTION

In our daily life, accidents occurring frequently might be turning into a disaster. Crashworthy structures and protective equipment such as body armors/helmets, etc. are substantial systems to shield humans and/or sensitive payloads. These protective systems minimize safety concerns and are responsible for withstanding several static and dynamic forces, including impact, compression, bending, and vibration. These systems aim to absorb energy before transferred to humans or payloads. The safety levels could be quantified by the energy absorption capabilities of such structures [1]. Therefore, innovative energy-absorbing material approaches focus on enhancing safety and minimizing the risk of catastrophic failure. Lately, novel polymeric foams with reinforcements are found to be offering substantial potential in energy absorption with their cellular structure, high surface area and stress transfer, and viscoelastic properties [1–3].

In various protective components such as helmets and armors, sandwich composites are the major structures for the purpose of energy absorption capability with the core materials and the face sheets. Conventional approaches with honeycomb geometries face several challenges due to a lack of sufficient contact area leading to face sheet delamination and moisture accumulation [4]. Thus, polymeric foams over conventional honeycombs can offer crack growth resistance and multidirectional load-bearing capability because of their cellular characteristics. Moreover, novel polymeric foams are widely studied materials for safety concerns that provide excellent bonding with face sheets owing to their high surface area and stress transfer, viscoelastic properties, and energy absorption capabilities.

1.1 Polyurethane Foams

Among several polymeric foams, polyurethane (PU) foams stand out by presenting high strength, energy absorption lightweight characteristics, ease of manufacturing, and tailorability [2, 5, 6]. PU is a particular polymer group that stands out with its unique chemistry which also has a potential to fill the vacancies between rubbers and

plastics [2, 7]. PU is used in various applications such as liquid coatings, elastomers, paints, elastic fibers, insulators, and foams. PU and its variations generate versatile materials while attracting researchers from different fields since their properties can be improved with an adequate selection of process parameters [8]. One of the most preferred and utilized forms of PU is foam structures [7]. PU foams demonstrate a wide range of densities between 20 kg/m^3 and 3000 kg/m^3 [9]. Depending on their formulation, PU foams could maintain their properties up to 135 °C which makes them, suitable for sandwich composites produced with prepreg face sheets [10].

PU foams are synthesized from two main ingredients, polyol, and isocyanate, while additional additives such as blowing agents, flame retardant agents, chain extenders, and catalysts could be added to achieve desired properties [11]. PU foams could be classified as flexible and rigid foams in terms of their mechanical behavior and cell morphology. The reaction of hydroxyl groups of polyol and functional groups of isocyanate produce urethane bonds and the blowing agent dissipates gas, forming the foam structure. The reaction is demonstrated in Figure 1.1. In the final product properties, usually, softness and flexibility are associated with polyol while hardness and stiffness arise from isocyanates and low molecular weight chain extenders content [12]. Furthermore, catalysts provide a fast reaction rate for the synthesis while enabling it to take place at lower temperatures. One of the control methods for foam formation is the selection of the blowing agent which supports the adjustment of porous (cellular) structure and their physical properties [2, 13–15].

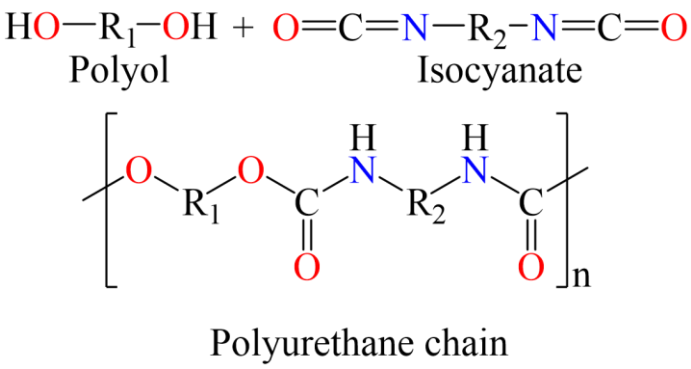

Figure 1.1: Polyurethane chain formation from polyol and isocyanate.

1.2 Structure-Property Relationship of PU Foams

The physical and mechanical properties of foams are highly related to morphological parameters [15–17]. Foam density, cell edge length, wall thickness, edge length to wall

thickness ratio, and cell density are the prominent parameters affecting the properties of PU foams [18, 19]. Cell edge length and cell wall thickness are demonstrated in Figure 1.2. Load-bearing capabilities of cellular structures increase with increasing cell density and thickness to length ratio. Cellular structure formation is affected by nucleation and growth kinetics [18, 20, 21]. Sung et al. reported that higher reactivity catalysts supplied a fast reaction rate, caused finer cells, and increased energy, sound absorption as well as compression strength [22]. Chen et al. reported that in closed-cell foams, increased cell sizes lead to a 25% decrease in compressive strength and slightly reduced shear strength (6%) while other parameters such as cell density and cell wall thickness were kept constant [23]. PU foams can typically be customized by either optimizing the process parameters or adding nano and/or micro-sized reinforcing agents for functionality that brings uncommon properties [24–26]. Besides, nanoparticle inclusion along with process parameter optimization could provide enhanced mechanical properties with multifunctionality where they act as nucleation points and provide reduced cell edge length and increased cell wall thickness and cell density, positively affecting mechanical properties [27–29].

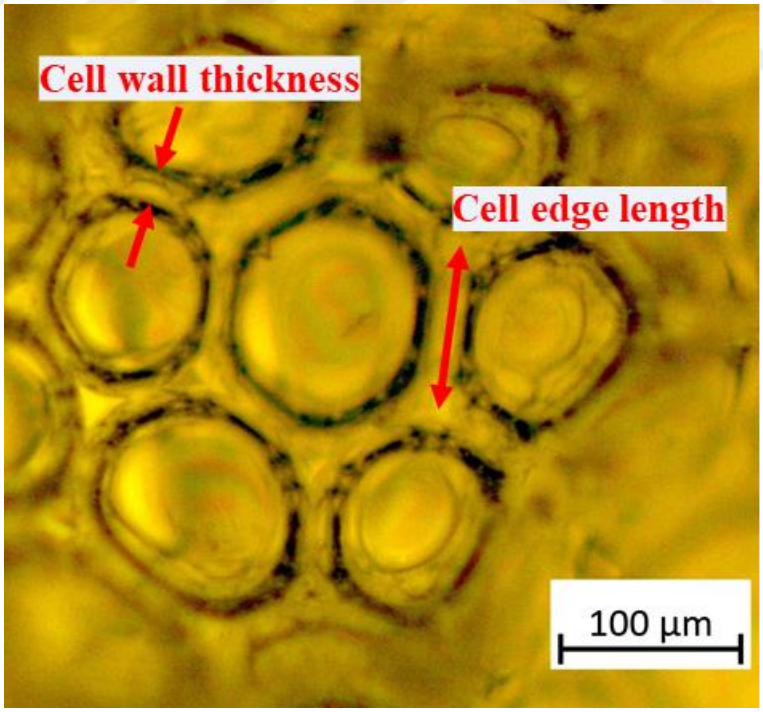

Figure 1.2: Microstructural parameters of a PU foam shown on an optical image.

According to a study conducted by Yan et al., the addition of 0.3 wt.% of graphene nanosheets into rigid PU foam led to a reduction in cell size by 12.1% and an increase in cell density by 47%. This resulted in a significant enhancement in the compressive

strength and modulus of the foam, with increases of 32% and 36%, respectively [30]. Saha et al. reported that 1 wt.% carbon nano fiber (CNF) reinforced rigid PU foams demonstrated an 85.9% higher tensile modulus and 40% higher compressive modulus. The enhancement in the mechanical properties originated from modifications in the microstructure of the foam. As a result of this CNF reinforcement, the authors obtained 11.3% lower cell sizes and 44.8% higher cell density [31]. Mahfuz et al. reported that it is possible to achieve 30% and 62% improvements in Young's modulus and flexural strength, respectively, with the addition of 3 wt.% TiO_2 nanoparticles in PU foams. They also observed 7% enhancements in decomposition temperature [32]. Xu et al. investigated the integration of organoclay nanoparticles to PU foams and found that compressive and tensile strength values were increased by 152% and 110%, respectively, whereas the cell size was reduced by 61% [33]. Hence through a tailored microstructure, PU foams can be customized for protective systems where energy dissipation mechanism needs to be further investigated.

1.2.1 Energy Absorption Mechanism and Measurement Techniques of PU Foam

Crashworthy structures such as PU foams, encounter different loads and expose external energy due to applied loads. The mission is to minimize the effect of these loads which can be possible with the absorption of applied energy. The applied energy is released as deformation of cells, friction, and heat [34, 35]. The difference between applied energy and collected energy is specified as absorbed (dissipated) energy. Energy absorption capabilities of PU foams vary depending on the mechanical loading conditions such as compression, cyclic compression, and dynamic mechanical forces. Therefore, potential forces should be considered according to the application area, and energy absorption capabilities are evaluated under these loads. Compression, cyclic compression, and dynamic mechanical forces play a crucial role in optimizing the performance of the structure.

1.2.1.1 Energy absorption and the compressive response of PU foam

In cellular structures such as PU foams, the compressive response of the material could be divided into three distinct regions that areas elastic, plateau, and densification regions [36]. The typical compressive response of PU foam under the stress-strain curve is shown in Figure 1.3. Energy dissipation mechanisms could be explained by

motions of cell walls. Under compression, in elastic region cell walls bend, then buckle in plateau region, which is followed by collapse [37, 38]. During the deformation of cells under compression, interfacial frictions between PU chains, filler-filler, and PU-filler mechanisms come into play, resulting in energy loss [39–41]. Absorbed energy could be calculated from area under compression curve [42]. Thus, higher strength which means higher load bearing capacity, acquires higher energy absorption under a single compressive load.

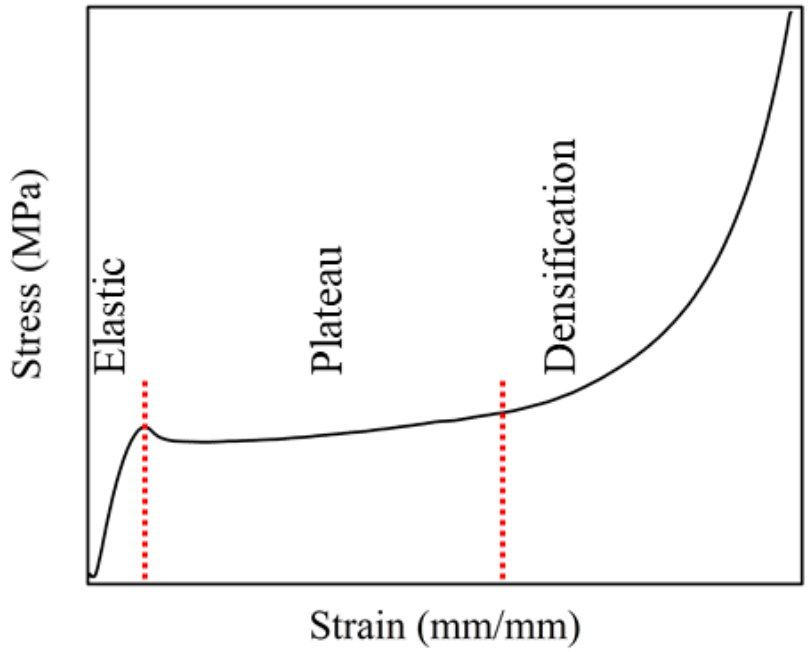

Figure 1.3: Typical compressive response of PU foam indication three different regions.

1.2.1.2 Energy absorption of PU foam under cyclic compression

Under cyclic compression, compressive loads are applied periodically with a constant strain rate or stress amplitude. In each cycle loading and unloading curve differ from each other due to the viscoelastic and deformation features of the foams. The area between the loading and unloading curves is a measure of the absorbed (dissipated) energy and named as the hysteresis area. These calculations directly express the energy absorption of foams. The units of hysteresis area are usually expressed in Joules per cubic meter and depend on the units of the stress-strain elements. Hysteresis area is used to quantify the amount of energy dissipated as heat within a given volume of material during each loading cycle. Energy absorption capabilities could be quantified by different approaches such as loss factor (η) and energy loss coefficient (ELC) [39, 40].

Loss factor which is also named as loss coefficient or loss tangent sometimes, is equal to the ratio of absorbed energy to the maximum potential energy during a cycle [43–46]. On the other hand, ELC can be calculated by dividing the hysteresis area by the area under loading curve [39, 47, 48]. Formulations of loss factor and ELC are given in equations 1.1 and 1.2, respectively.

$$\eta = \frac{\Delta W}{\pi U} \tag{1.1}$$

$$ELC = \frac{Hysteresis\ Area}{Area\ under\ loading\ curve}\ x\ \%100 \tag{1.2}$$

Where ΔW and U denote the hysteresis area and the maximum potential energy which is the area under an imaginary line that passes between loading and unloading curves. Loading and unloading curves and maximum potential energy under cyclic compression test of a typical PU foam are demonstrated in Figure 1.4. These measurements are important in applications where energy-absorbing materials are used, as the ability to dissipate energy efficiently is critical in reducing the impact of applied forces on structures and components [39, 43–47].

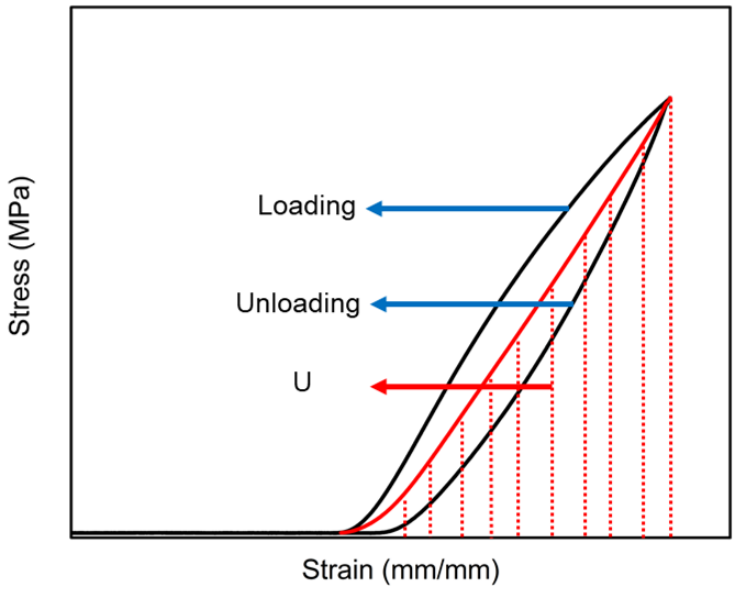

Figure 1.4: Loading and unloading curves and maximum potential energy under cyclic compression test of a typical PU foam.

1.2.1.3 Energy absorption of PU foam under dynamic mechanical analysis

Energy absorption and viscoelastic properties could be measured with dynamic mechanic analysis under different loads such as bending, tension, shear, and

compression. In dynamic mechanical analyses, periodic loads are applied with a sinusoidal waveform, periodically displacing the sample [44, 45]. If the sample exhibit pure elastic behavior, the peak of force and displacement curves are observed at the same time. In viscoelastic materials, there is a difference between these peaks which is named as phase angle (δ or Δ). The larger the phase angle, the much delayed the displacement peak response is relative to the force peak, showing higher energy dissipation by the material. Force and displacement curves of a viscoelastic material depending on the time and phase angle are demonstrated in Figure 1.5 [44]. From the force and displacement curves, storage and loss moduli values could be calculated. Storage modulus represents the stored potential energy during a cycle, hence the elastic response whereas loss modulus represents the absorbed (dissipated) energy during a cycle. Additionally, tangent δ which is named as loss tangent or loss factor is obtained from the ratio of loss modulus to storage modulus and demonstrates energy absorption capabilities of the materials [44, 45].

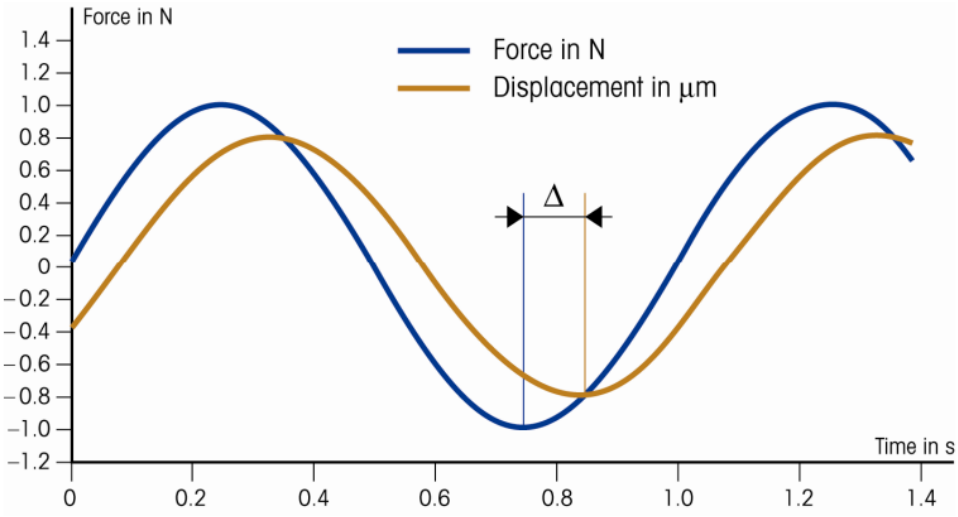

Figure 1.5: Force and displacement curves of a viscoelastic material under dynamic load [44].

1.3 PU Foams for Energy Absorption Structures

The utilization of PU foams for energy absorption purposes has been widely researched and demonstrated through various examples that incorporate carbon-based nanomaterials such as carbon nanotube (CNT) and graphene, and neat PU foam [49–52]. Yang et al. designed a PU foam integrated hybrid composite system for railway trains in order to minimize crash energy [53]. The hybrid composite system which is demonstrated in Figure 1.6, consisted of carbon fiber reinforced outer tube, PU foam,

and an inner aluminum tube. Liu et al. reported that PU foam integration into aluminum foam gained recoverable deformations along with the viscoelastic characteristics of the foam and demonstrated higher energy dissipation and loss factor values than aluminum foam under cyclic compression test [46].

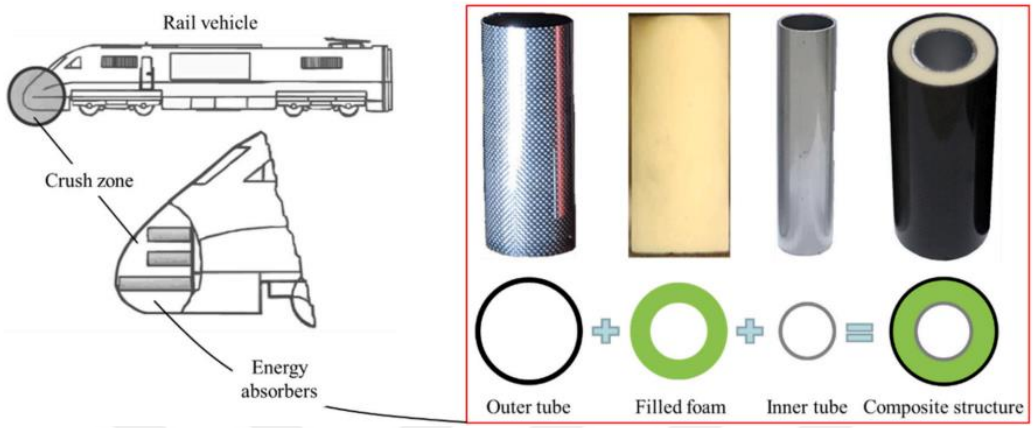

Figure 1.6: PU foam integrated hybrid composite system for railway trains [53].

Bhinder et al. investigated the effect of strain and strain rate on the energy dissipation properties of neat and CNT-doped PU foams under cyclic compression tests [39]. Cell density increased and cell diameter decreased with increasing CNT content. The performed compression tests with different strain rates clearly represent the elastic, plateau, and densification regions in Figure 1.7. The results revealed that stress values increase with increasing strain rate. This behavior was explained by the morphological characteristics of PU foams. The closed-cell structure keeps air within the cells which is released under the pressure generated by the applied load. Due to the gaseous and viscous nature of the air, when the applied strain rate or strain increases, stress values also increase as well because of the increased air pressure demonstrating higher resistance to deformation [39, 54, 55].

Single and 10-cycle cyclic compression loads under different strain rates and strains were applied in order to understand the energy absorption properties in the elastic, plateau, and densification regions. The single-cycle compression test results are demonstrated in Figure 1.8. They reported that 2.3 wt.% oxidized CNT-doped PU foams demonstrated higher energy dissipation at low strains, i.e. elastic region. However, when higher strains were under investigation, the doping resulted in lower energy dissipation capabilities. They reported that the main factor of energy dissipation

at high strains is the collapse of cells, while at low strains, filler-filler and PU-filler interactions are the dominant factors [39].

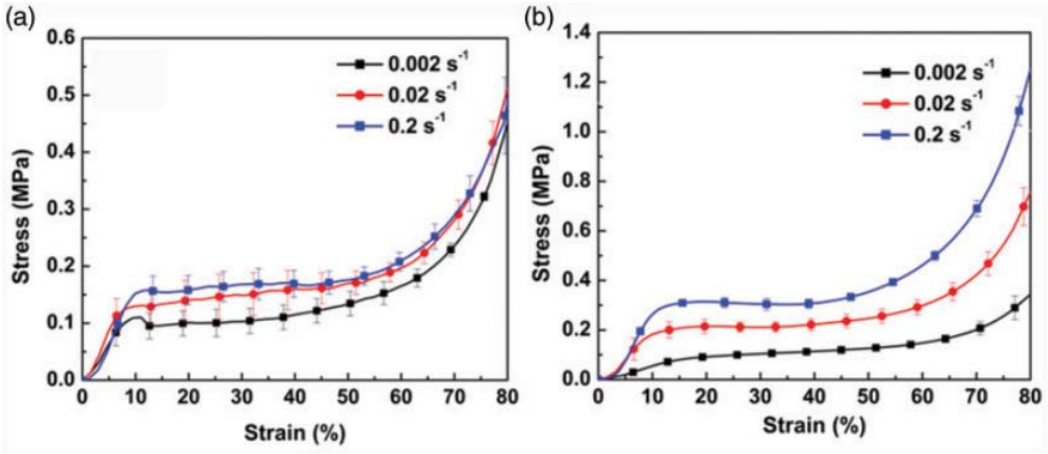

Figure 1.7: Compressive response of a) neat and b) 2.3 wt.% oxidized CNT-doped PU under different strain rates [39].

In another study, Lu et al. investigated the effect of graphene oxide (GO) and external PU dispersion coating on the energy dissipation of flexible PU foams. It was concluded that the interaction between GO-GO and GO-foam provided energy loss where at higher loadings of GO beyond 0.2 wt.%, the sliding of the GO layers due to Van der Waals interactions disappeared with the highly overlapped GO [41].

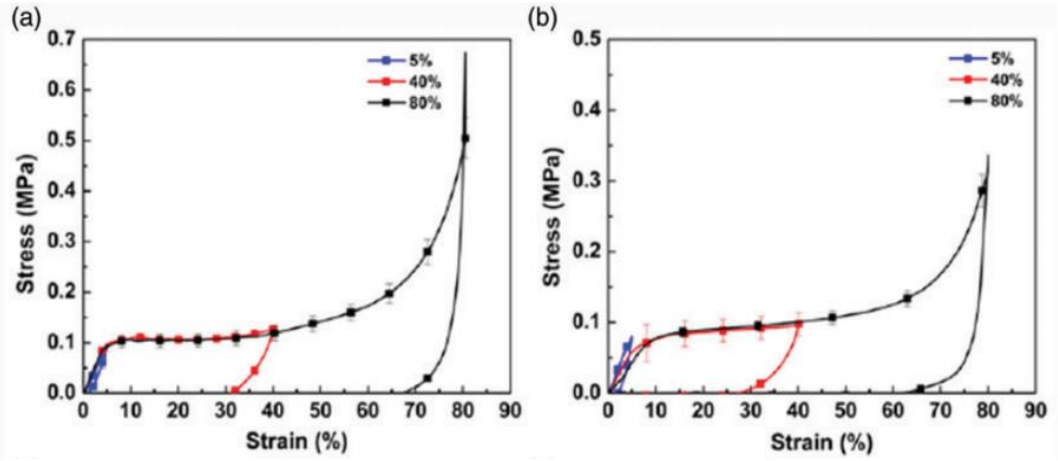

Figure 1.8: Cyclic compressive response of a) neat and b) 2.3 wt.% oxidized CNT-doped PU under different strains at 0.002 s^{-1} [39].

Even though carbon-based nanostructures such as CNTs and graphene have been widely studied as reinforcing agents in polymeric foams in order to enhance energy absorption capabilities, still efforts are needed to define the role of other nanomaterials

such as shear thickening fluids (STFs) due to excellent energy absorption characteristics.

1.4 Shear Thickening Fluids as additives for energy absorption applications

STFs are non-Newtonian fluids demonstrating strong toughening behavior under applied shear and are used in several applications where energy absorption is required. STFs are composed of colloidal solid particles such as silica or styrene-acrylate copolymer particles and the liquid phase, where the flow properties are independent from applied shear. At low shear rates, the solid particles within STFs are oriented, STFs flow easily, thus viscosity is rather low. The decrease in the viscosity under the applied shear rate is called shear thinning behavior. Beyond a critical shear rate, oriented solid particles form hydroclusters due to the applied shear rate and particle interactions, which resist flowing, in return viscosity increases drastically. The shear rate where the viscosity becomes minimum is called the critical shear rate. The shear thickening phenomenon is reversible when the applied shear is removed. Flow behavior of STFs is demonstrated in Figure 1.9. The ratio of minimum to maximum viscosity is referred to as the thickening ratio. Viscosity, critical shear rate, and thickening ratio are the essential performance parameters of STFs for energy absorption capabilities [56–60].

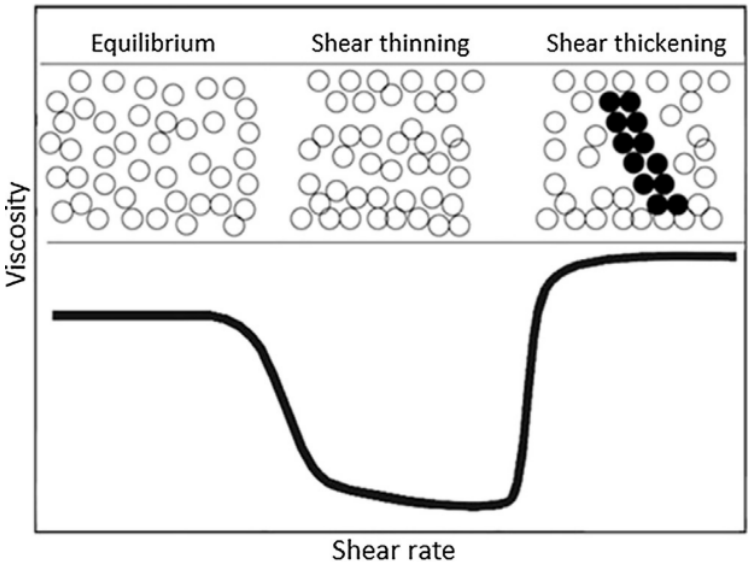

Figure 1.9: Flow behavior of STFs, under applied shear [60].

Three different approaches exist in the literature in order to understand shear thickening behavior: order-disorder theory, hydrocluster theory, and contact rheology model. According to order-disorder theory, the particles are coherent, such as layer by layer below the critical shear rate. Beyond that, the layers become disordered due to hydrodynamic forces, and the viscosity of the suspension increases dramatically [61]. According to hydrocluster theory, hydrodynamic forces are higher than the particle interactions, such as repulsive forces beyond the critical shear rates, and particles formed as hydroclusters thus, the suspension exhibit thickening behavior [62]. The contact rheology model explains the thickening with contact forces between particles in the suspension providing thickening after the critical shear rate [60, 63, 64]. Flow behavior of STFs could be influenced by several parameters such as particle size, shape, concentration, temperature, and chemical composition of liquids and solids. Yu et al. investigated the effect of silica particle size and concentration on the STF suspensions. The particle sizes were 15, 30 nm and 2, 5, 10 μm, and weight fractions varied from 5% to 70%. The flow behavior of the suspensions is demonstrated in Figure 1.10. The particles were dispersed in Polyethylene glycol (PEG) with using a magnetic stirrer. They reported that hydroxyl groups of silica and PEG interact with each other and form hydrogen bonds which provided stability of STFs. After the critical shear rate, the hydrogen bonds between the particles in the STF broke, and solid particles formed into clusters which led to shear thickening. Due to the increasing shear rate, the clusters were destroyed, after shear thickening behavior, and shear thinning was observed again. The suspensions exhibited shear thickening behavior depending on the concentration of the silica particles. Shear thickening could be observed after 10 wt.% 15 nm silica or 60 wt.% 2 μm silica particles addition. Thickening behavior increased with increasing silica concentration for the same particle size. It can be clearly seen, in Figure 1.10, that under the same concentration, STF with smaller particle size demonstrates higher thickening ratio and lower critical shear rate. At low concentrations, the reduction of solid particles results in a weakening of the interactions between silica and PEG, and the viscosity of the fluid and shear thickening response decreases accordingly. STFs produced with smaller particle sizes exhibited shear thickening prior to the larger ones. Viscosity and shear rate sensitivity increased with decreasing particle size. The authors explained this situation by stating that smaller particles could interact more effectively with each other. The study indicated that, compared to silica nanoparticles, silica microparticles were less stable

and more prone to sedimentation over long periods of storage. This finding has implications for the use of these materials in various applications and highlights the importance of understanding the properties of different particle sizes and concentrations to optimize performance and ensure stability over time [65].

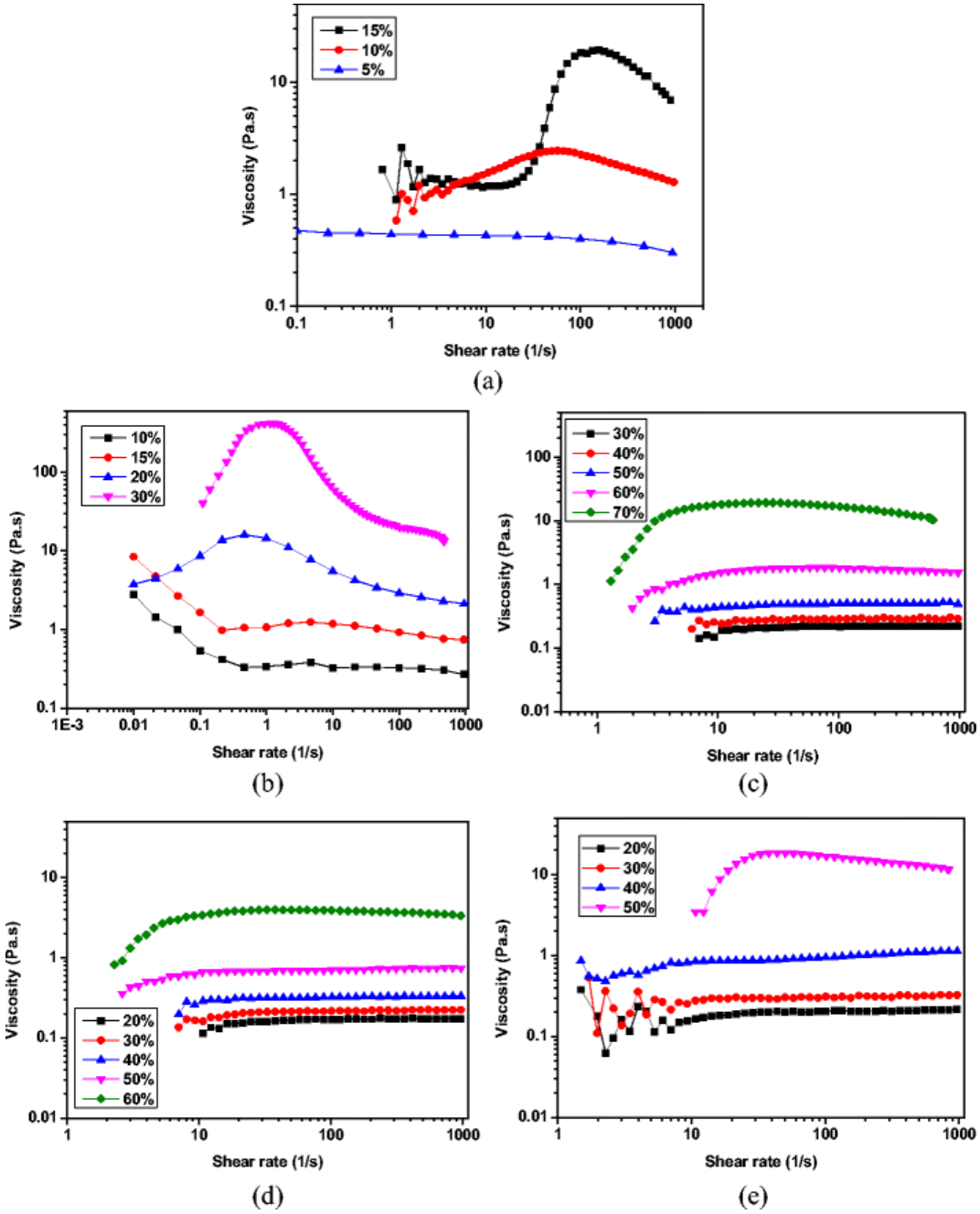

Figure 1.10: Flow behavior of STFs with different concentrations and particle size: a) 15 nm, b) 30 nm, c) 2 µm, d) 5 µm, e) 10 µm [65].

STFs are integrated into several structures, such as aramid fiber, fabrics, honeycombs, rubber, and organogel for energy absorption and safety in order to enhance energy absorption capabilities under different loads [66–73]. PU foams have superior energy

absorption and thermal insulating properties hence the integration of STFs into rigid PU foam could stabilize STFs flow behavior, prevent leakage, and achieve higher energy absorption for PU foam. Also, the formation of hydrogen bonds among the PU chains is known to enhance mechanical properties such as strength and modulus [33, 74–77]. STF integration into PU foam could be improved mechanical properties due to enhanced hydrogen bond formation with silica and hydroxyl groups in their structure and modify nucleation and growth kinetics. Caglayan et al. obtained 29% improvement in specific compressive strength with 1 wt.% STF addition into PU foam and reported that the energy absorption capability of STF integrated PU foam sandwich composites increases with increasing silica content under impact loads [57]. Fu et al. studied the influence of temperature on the rheological and energy absorption characteristics of STFs under impact loads and it was revealed that the response time and penetration depth increase with increasing temperature [56]. Soutrenon et al. showed that STF-impregnated open-cell foams with silicone composite pads can absorb up to 85% higher energy compared to pure silicone [58]. Moreover, Haris et al. investigated STF impregnated flexible PU foams and reported that STFs did not change quasi-static compression performance, whereas under impact tests, peak force was reduced by 46% with STFs filling [59].

1.5 Purpose of the Thesis

PU foams are used as core materials in composites applications with various purposes such as insulation, sound absorption, load bearing element, and energy absorber or damper. According to former studies, the properties of the foam are related to their cellular structures which can be tunable with nanoparticle integration. Possible enhancements in their properties provide more safety and sustainable life for humanity. For instance, reduced weight provides lower energy consumption during the processing and service period. Improvement in the energy absorption and mechanical properties of PU foams contributes to reliable structures. Also, STFs are used for energy absorption applications due to their strong toughening behavior for protective equipment. To the best of our knowledge, only a small number of studies focus on the reinforcing PUs using STFs with an aim to improve the mechanical properties.

This thesis aimed to investigate the mechanical and energy absorption properties of STF-reinforced PU foams while discussing the potential solutions to overcome the

process-related problems. Research road map of the thesis was illustrated in Figure 1.11. Initially, STFs were produced with spherical and fumed nanosilica particles and different weight fractions up to 30 wt.% in order to optimize shear thickening behavior. STFs were then successfully integrated to rigid PU foams at 0.5, 1, and 3 wt.%, and the morphological analysis was carried out by an optical microscope and scanning electron microscopy (SEM) to develop the microstructure-mechanical property relationship. Then, the mechanical properties of STF integrated PU foams were characterized by compression, cyclic compression tests, and dynamic mechanical analysis.

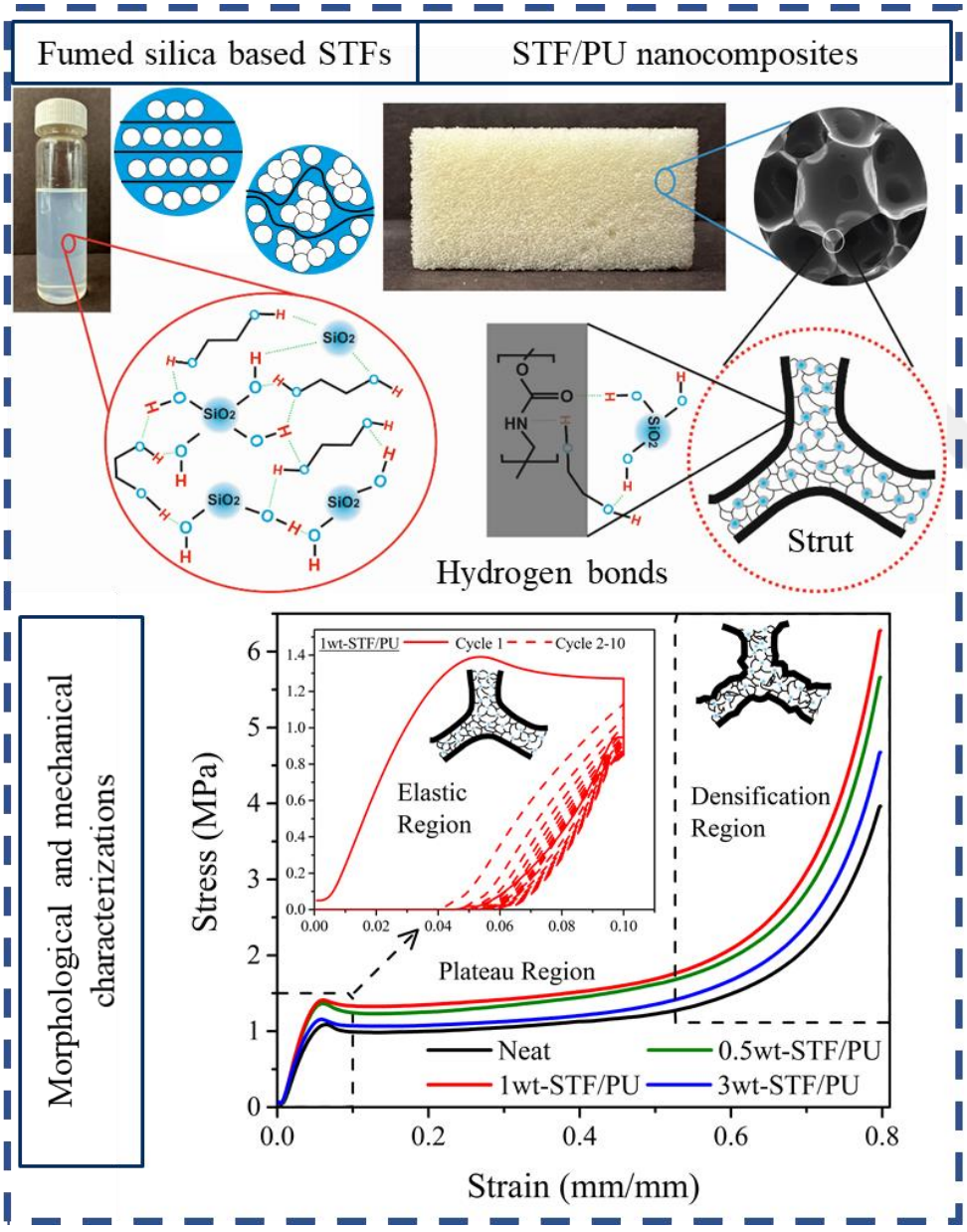

Figure 1.11: Fabrication and characterization of STF/PU foam.

This study consists of: introduction, materials and methods, results and discussion, and conclusion. In the introduction chapter, general knowledge about PU foam and their nanocomposites, the effect of morphological features on the mechanical properties of PU foam, energy absorption mechanism, and measurement techniques, rheological behavior of STFs, and utilization of PU foams for energy absorption purposes are reviewed. In the materials and method chapter, supplied raw materials, fabrication procedures, characterization methods, and test parameters are shared. Rheological analysis of produced STFs, the microstructure of neat and STF integrated PU foams, the results of compression, cyclic compression, and dynamic mechanical analysis tests in order to understand viscoelastic properties and energy absorption capabilities are discussed and presented in the results and discussion chapter. Summary of the thesis and the obtained experiences are shared in the conclusion chapter.

2. MATERIALS AND METHODS

2.1 Materials

PU foam was supplied by AKTIF POLIURETAN in two liquid forms: polyol and polymeric diphenylmethane diisocyanate (PMDI) where polyol consists of components as catalyst, stabilizer, blowing, and curing agents. The weight ratio of polyol and PMDI was 1:1.05, according to the manufacturer's formulation. The density of neat PU foam was 100 (±10) kg/m^3. Ethylene glycol (EG) was supplied from Sigma-Aldrich with a molecular weight of 62.07 g/mol, as a carrier fluid of STF. For the solid content of STF, amorphous fumed silica nanoparticles (AEROSIL 200) supplied as a dry powder with a particle size of 11 nm and surface area of 175-225 m^2/g from Evonik and amorphous, spherical silica nanoparticles with 13-22 nm particle size and 165-195 m^2/g specific surface area were supplied from Nanografi Ltd. Co., Turkey.

2.2 Fabrication of Shear Thickening Fluids

STFs were prepared from amorphous fumed silica nanoparticles and spherical silica and EG. Silica nanoparticles were dried for at least 2 days at 150 °C in order to eliminate moisture. Then, the dried silica nanoparticles were dispersed in EG using a constant mechanical mixing rate of 500 rpm to form the concentrated colloidal suspensions. The mixture was sonicated for 90 s with 30% amplitude, using a horn sonicator after 13 wt.% of silica nanoparticles were added. Afterwards, the silica nanoparticles were continuously added to the mixture in small amounts while being mechanically stirred which was followed by a 90 s sonication step to achieve higher concentrations. The process was performed for STF with various concentrations and optimized to achieve the best dispersion of silica nanoparticles within EG. The fabrication of STF was carried out with fumed silica concentrations at various weight fractions of 19, 22, 24, 26, and 28 wt.%, and 30 wt.% with spherical silica which was dispersed in EG. The shear thickening behavior of STFs is investigated as a function of silica content and particle geometry through rheological analysis. The summary of

the fabrication details of STFs with different silica nanoparticles and weight fractions is given in Table 2.1 while the fabrication procedure and the corresponding testing are illustrated in Figure 2.1.

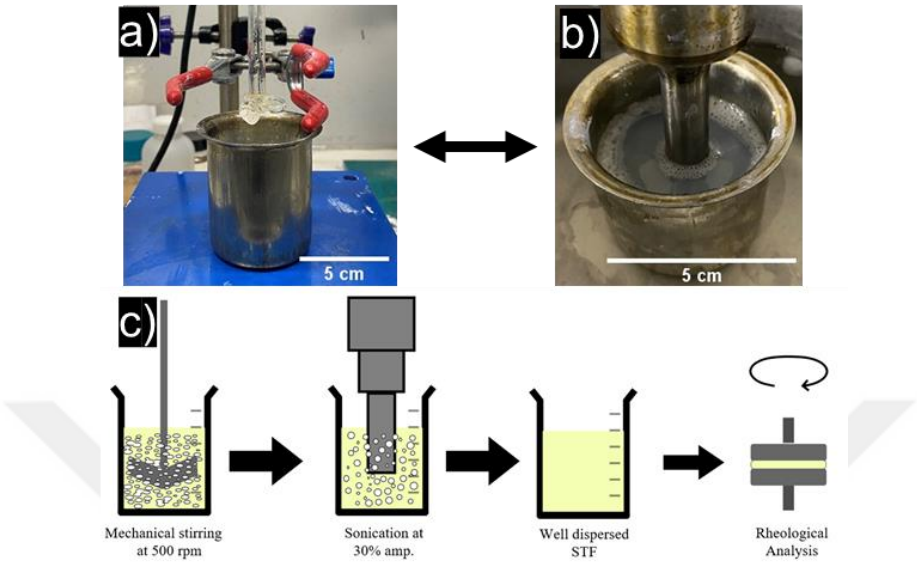

Figure 2.1: STF fabrication: a) mechanical stirring b) Sonication c) Illustration of fabrication and characterization of STF samples.

Table 2.1: Detailed fabrication procedure for each STF sample, indicating the stirring time, sonication count, and the sample coding based on the silica weight fraction in EG.

Sample coding	Silica type	Silica weight fraction in EG (%)	Stirring time (h)	Sonication count*
STF-19	Fumed	19	2.7	3
STF-22		22	3.7	4
STF-24		24	4	5
STF-26		26	4.2	5
STF-28		28	4.8	6
STF-30-S	Spherical	30	5.2	7

** Each sonication interval was 90 s.*

2.3 Neat and STF integrated Polyurethane Foam Nanocomposites Fabrication

In this study, 4 different PU foams were synthesized with/without STF in order to understand the effect of STF integration. Initially, Polyol was mixed for 4.5 h by a mechanical stirrer (RW20 Basic, IKA) at 300 rpm, then PMDI was added and the mixture was stirred at 2000 rpm for 50 s. The mixture was then poured into a pre-

heated mold at 40 °C and left for foaming at room temperature for 15 min. Then, the foam was placed and cured in an oven at 40 °C for 24 h, and neat PU foam was obtained.

STF integrated PU foams (STF/PU) were prepared with contents of 0.5, 1, and 3 wt.% STF where the samples were coded based on their STF concentrations. For instance, PU foam with 1 wt.% STF content is coded as 1wt-STF/PU. While fabricating the STF/PU foams, polyol was chosen for the dispersion of STF since PMDI was not suitable as it would interact with hydroxyl groups in EG prior to the foaming procedure. First, STF and polyol were mixed by a mechanical stirrer operated at 300 rpm for 4.5 h. Then, PMDI was evenly mixed with polyol at 2000 rpm for 50 s. The summary of the fabrication details and further characterizations of STF/PU with different STF content are illustrated in Figure 2.2. The details of characterizations such as testing parameters and instrument details, and sample dimensions are shared in the following sections.

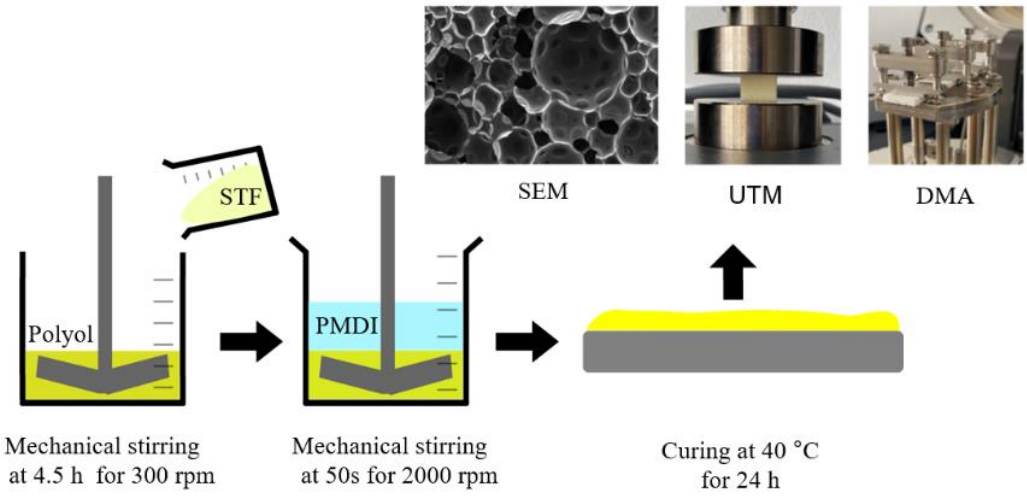

Figure 2.2: Fabrication and characterization of STF/PU samples.

2.4 Characterizations and Mechanical Tests

2.4.1 Rheological Analysis

Flow behavior of the as-prepared STFs was investigated by TA Instruments DHR-II rheometer using 25 mm parallel plate geometry and 0.2 mm gap at room temperature. 100 s^{-1} pre-shear was applied for 20 s and then waited for 60 s in order to stabilize the samples. The shear rate was varied between 0.1 and 3000 s^{-1} using the logarithmic flow sweep mode with 10 s averaging time for each step.

2.4.2 Microstructural and morphological characterization

The cellular structure of the neat and STF/PU foams was investigated by optical micrographs and scanning electron microscopy (SEM). Cell edge lengths (l), cell wall thicknesses (t), and cell densities of the neat and STF/PU foams were measured by using ImageJ software and examined to establish a microstructure-property relationship. Cell densities were calculated by equation 2.1 from SEM micrographs where n was the number of cells, A is the area of the micrograph in cm^2 and M is the magnification factor of micrograph [32, 78].

$$N = \left(\frac{nM^2}{A}\right)^{3/2} \tag{2.1}$$

2.4.3 Quasi-static compression and cyclic compression tests of PU foams

Quasi-static compression tests were performed by Shimadzu universal test machine (UTM) with a 50 kN load cell. The foams were milled by a CNC machine and specimen dimensions were determined to be 30x30x15 mm^3 which is demonstrated in Figure 2.3 in accordance with ASTM C365-16. The tests were conducted in a strain-controlled mode with maximum strains of 10%, 40%, and 80%. The tests were performed on at least 3 specimens for each type and condition. The applied strain rates were also chosen as 0.002, 0.02, and 0.2 s^{-1} to evaluate the effect of the strain rate on the mechanical properties. The specimens were also investigated for their energy absorption capabilities via cyclic compression tests. The cyclic compression tests adopted the same strain levels and strain rates as quasi-static compression tests and 10 cycles per specimen were performed with 5 s pause at the maximum strain for each cycle.

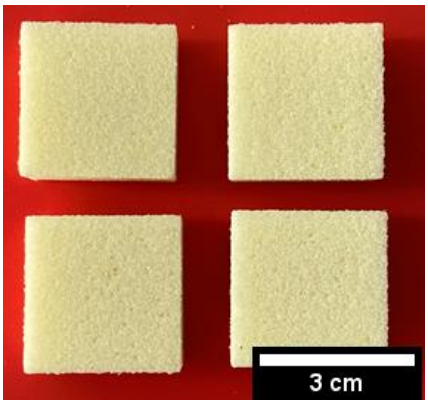

Figure 2.3: Prepared neat PU samples for compression test.

2.4.4 Dynamic mechanical analyses of PU foams

Dynamic mechanical properties of the neat and STF/PU foams were measured by TA Instruments DMA-850. The tests were carried out using a dual cantilever fixture under flexural loading. Specimen dimensions were determined to be 65x13x3 mm^3 under compliance with ASTM D5418-15. Initially, strain-sweep tests were performed to determine the linear viscoelastic region (LVR) and the applied oscillation displacement. Based on the determination of the LVR, the frequency sweep tests were performed between 0.1 and 10 Hz using 35 μm oscillation displacement.

3. RESULTS AND DISCUSSION

3.1 Rheological Properties of Shear Thickening Fluids

STFs were tested with the rheometer in order to investigate flow characteristics and optimize thickening behavior depending on solid content fraction and geometry. Shear thickening behavior was observed after 19 wt.% and 30 wt.% for fumed and spherical silica particles, respectively. Sample coding and composition details were shared in Table 2.1 in Chapter 2.

Viscosity vs shear rate graphs were created as shown in Figure 3.1 for STF-30-S (a) and STF-19 (b). Both samples exhibited shear thickening after the shear thinning regime. Fumed silica particles (STF-19) demonstrated dramatically toughening under applied shear. The viscosity increased from 0.33 Pa.s to 7.47 Pa.s which equals to 22.64 thickening ratio with 19 wt.% fumed silica content. On the other hand, spherical silica particles (STF-30-S) demonstrated a 2.95 thickening ratio and 2.94 Pa.s minimum viscosity. It can be clearly seen that silica surface properties dramatically affect the flow behavior of STFs.

This situation could be explained by the higher surface area providing higher hydrogen bonding capabilities with the carrier fluid [79]. Thus, shear thickening could be achieved a lower amount of silica particles with higher performance. According to these results, the usage of fumed silica particles could be enhanced the energy absorption capabilities of PU foam. Fumed silica particles have lower viscosity when compared to spherical silica particles, they can be processable conveniently and dispersible in PU foam.

Although spherical and fumed silica particles demonstrated shear thickening, fumed silica particles are more suitable for the purpose of this study due to the higher thickening ratio and low viscosity values. The following STFs were fabricated with fumed silica particles to optimize shear thickening behavior.

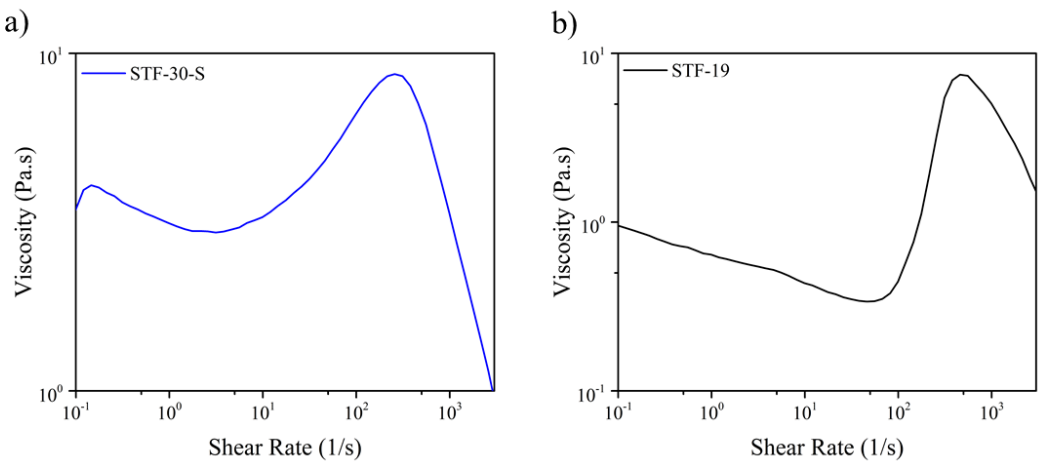

Figure 3.1: Flow characteristics of STFs with different silica geometry: a) spherical (STF-30-S) b) fumed (STF-19).

STFs were produced with the intent to optimize shear thickening fluid with 19, 22, 24, 24, and 28 wt.% fumed silica particles. After the 28 wt.% fumed silica, the produced suspensions tend to agglomerate and became inhomogeneous due to the higher surface area of fumed silica particles. Samples were coded as according to their fumed silica weight fractions. Flow characteristics of STF with different fumed silica weight fractions are demonstrated in Figure 3.2 and the obtained results are shared in Table 3.1. Shear thinning and shear thickening phenomena were observed in each sample. Initially, particles were oriented, due to applied shear and hydrogen bonds between EG and fumed silica. After around 46 s^{-1}, the particles formed into hydroclusters which resist flow, and viscosity increased dramatically. The transition from shear thinning to thickening, depending on the applied shear rate is called critical shear rate. After the shear thickening, shear thinning was observed again due to destroying of hydroclusters and could not resist to flow. Viscosity values increased with increasing fumed silica content and critical shear rates were similar regardless from fumed silica weight fraction. Thickening ratio increased with increasing fumed silica content until STF-26. The slight decrease in the maximum viscosity and thickening ratio of STF-28 could be explained by excessive silica content. Excessive silica loading could be caused agglomerations which crumble under the applied shear and lead to a decrease in the viscosity [80]. Overall, the results indicated that the maximum thickening ratio was obtained with STF-26. Considering the great change in the viscosity levels from 0.74 to 50.07 Pa.s with the applied shear, it was concluded that STF-26 was the most suitable suspension for the integration into PU foams.

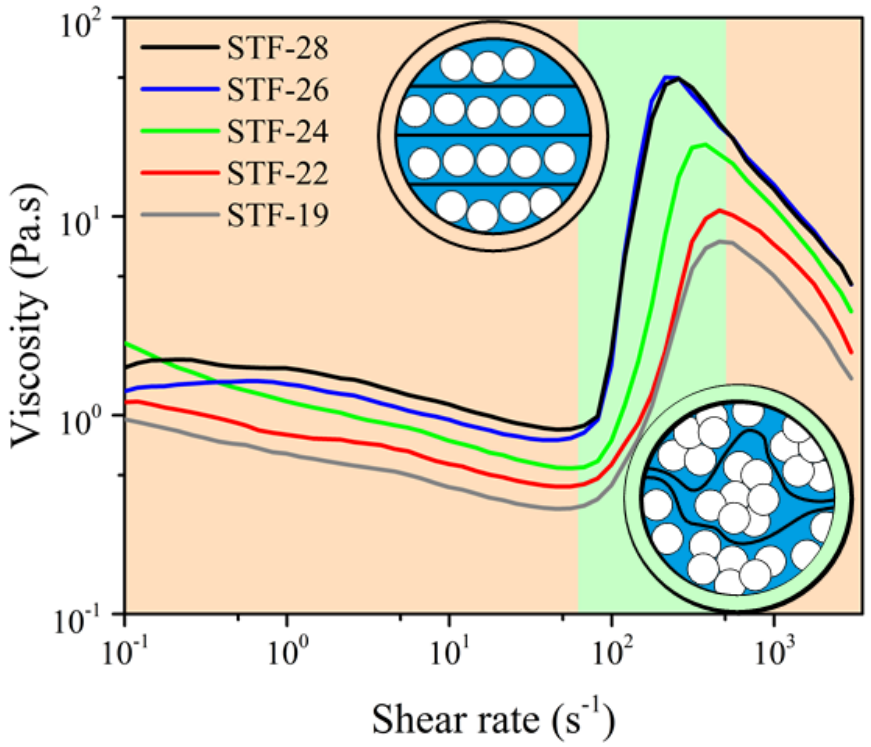

Figure 3.2: Flow characteristics of STFs with different fumed silica weight fractions.

Table 3.1: Rheological properties of STFs with different fumed silica weight fractions.

Sample	η_{min} (Pa.s)	η_{max} (Pa.s)	Thickening ratio (η_{max} /η_{min})
STF-19	0.33	7.47	22.64
STF-22	0.43	10.71	24.91
STF-24	0.55	21.91	39.84
STF-26	0.74	50.07	67.66
STF-28	0.84	49.42	58.83

Ensuring high-quality dispersions is crucial for accurate and reliable results. Also dispersion stability and shelf life being important considerations. Time-dependent tests were conducted to assess the dispersion stability of STF-26 before integrating it into PU foam, which is shown in Figure 3.3. The tests were carried out on the first, second, third, 16th, and 32nd days after fabrication, D1 corresponds to the fabrication day. STFs dispersion quality is vital for desired foam properties such as energy absorption, mechanical strength, and durability. A stable and homogeneous dispersion ensures uniform particle distribution throughout the foam matrix, enabling efficient stress transfer and reinforcing mechanical integrity. Deviations in dispersion quality could be led to inconsistent and suboptimal foam characteristics. STF-26 has kept their

properties for more than 1 month. Therefore, the ability of dispersion like STF-26 to retain its properties over time and under varying conditions is essential for accurate and reliable results, accounting for storage. High-quality dispersion is essential for sustainability as it enables the efficient utilization of resources and minimizes waste. By achieving uniform particle distribution and stability, dispersion quality ensures optimal performance and functionality, reducing the need for excessive material usage and improving the overall sustainability of processes and products.

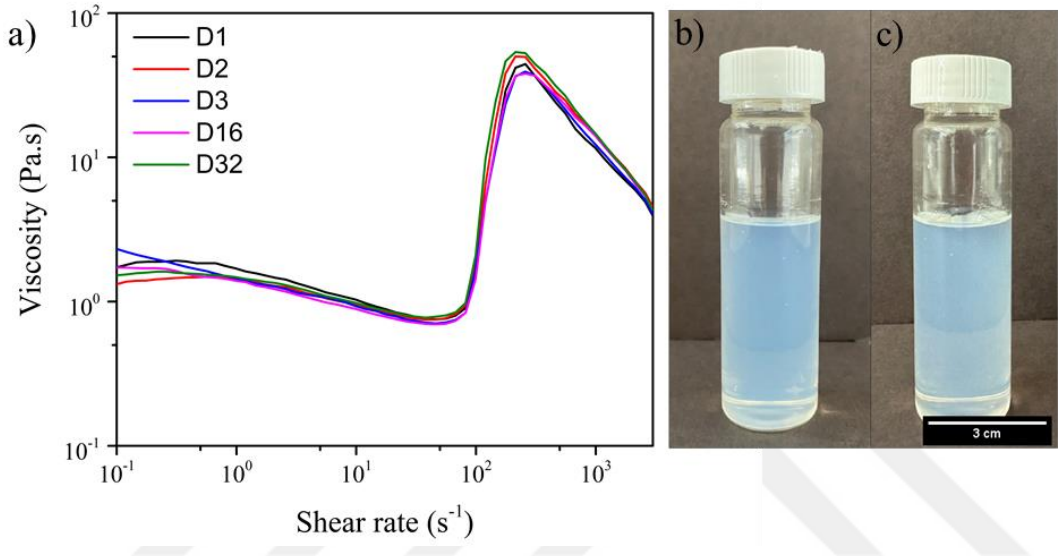

Figure 3.3: a) The rheological analyses of as-prepared STF-26 on different days after the fabrication and the dispersion stability of STF-26, on b) the fabrication day (D1), and c) the 32nd day (D32).

3.2 Microstructural and Morphological characterization of PU foams

Morphological properties of neat and STF-26 integrated PU foams were investigated. STF-26 was chosen to be the only suspension to be integrated into PU foam because of its excellent thickening behavior and stability. The microstructural and morphological observations of 0.5 wt.%, 1 wt.%, and 3 wt.% STF-26 integrated PU foams were carried out to investigate the changes within the microstructure. The micrographs are shown in Figure 3.4 which was obtained from the optical microscope, and Figure 3.5 which was obtained from SEM. Especially, the nanomaterial addition is known to trigger heterogeneous nucleation yielding disproportional cell sizes [81, 82]. To avert such occasions, the dispersion quality is of utmost importance and to evaluate dispersion quality, morphological characterizations are indispensable.

Using the ImageJ software, the micrographs were evaluated to determine the microstructural properties of the foams. Density, cell features such as edge length, wall thickness, density, and thickness to length ratio (t/l) of the as-prepared foams are presented in Table 3.2.

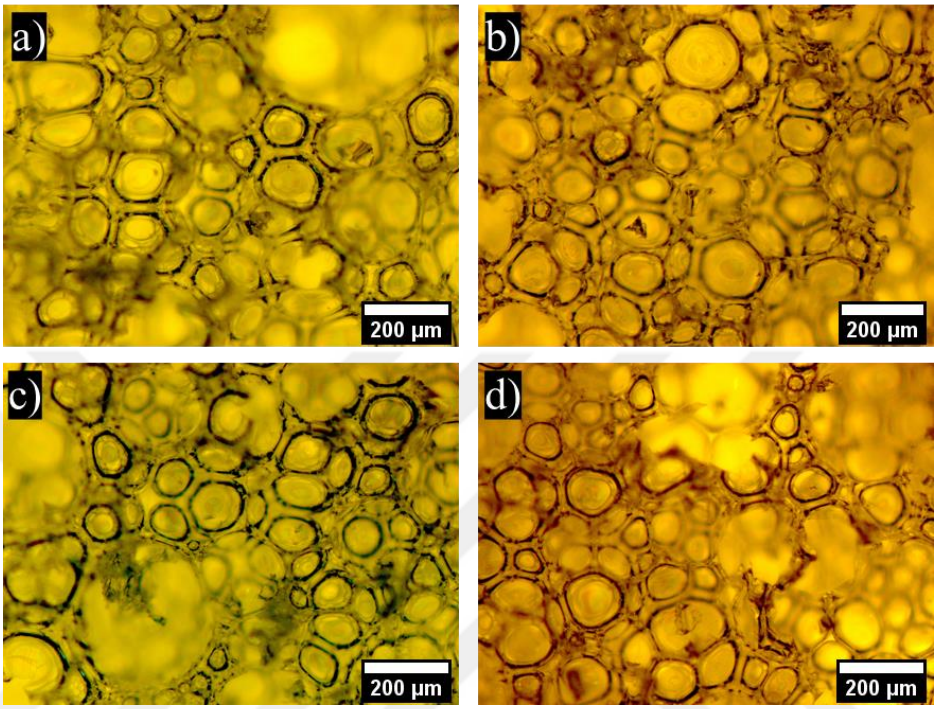

Figure 3.4: Optical microscopy images of PU foams at 5x magnification: a) neat, b) 0.5wt-STF/PU, c) 1wt- STF/PU, and d) 3wt- STF/PU.

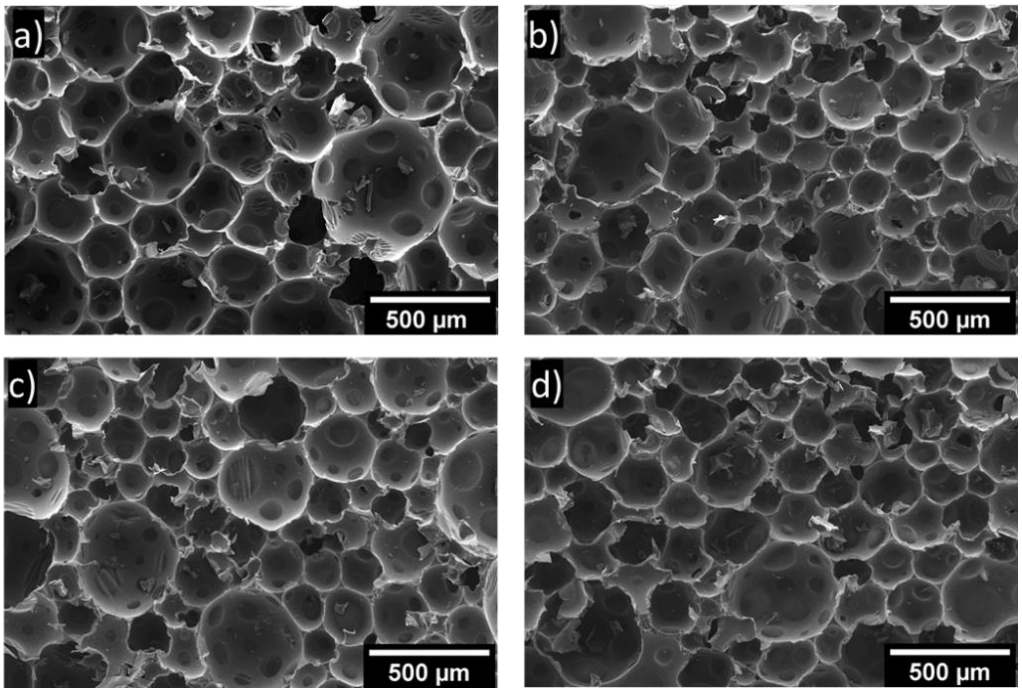

Figure 3.5: SEM images of PU foams at 200x magnification: a) neat, b) 0.5wt-STF/PU, c) 1wt- STF/PU, and d) 3wt- STF/PU.

Table 3.2: Densities and cell properties of PU foams.

Sample	Density (kg/m^3)	Cell edge length (μm)	Cell wall Thickness (μm)	t/l	Cell density ($\times 10^4$ cells/cm^3)
Neat	94.98 ±0.26	275.24 ±71.32	20.46 ±5.29	0.07	3.25
0.5wt-STF/PU	113.61 ±0.96	224.60 ±85.77	27.38 ±4.74	0.12	6.46
1wt-STF/PU	114.14 ±1.42	217.83 ±74.32	28.01 ±6.36	0.13	5.81
3wt-STF/PU	102.79 ±0.50	250.70 ±74.14	23.80 ±6.44	0.09	4.87

Typically, the cell density and the t/l ratio are accepted to be good indicators for the mechanical properties of rigid foams [18, 19]. Based on the evaluation of such properties revealed that the addition of STF into PU foams increased the cell density and t/l ratio in all of the samples. The maximum increase in the cell density as high as 78% was achieved in 0.5wt-STF/PU which was accompanied by a 71% increase in the t/l ratio. Such increases suggest that more load-bearing elements per unit area are generated. The increase in the cell density could be attributed to the STFs acting as nucleation points in the cell formation process.

The results showed that the cell edge lengths were observed to be similar around 220 μm and due to the heterogeneous nucleation kinetics for 0.5wt-STF/PU and 1wt-STF/PU, no significant difference between these samples was observed. Neat and 3wt-STF/PU have higher cell edge lengths. The cell wall thicknesses and t/l ratios were increased with STF-26 integration until 1wt-STF/PU. 0.5wt-STF/PU and 1wt-STF/PU showed almost the same increase in the cell wall thickness whereas 3wt-STF/PU exhibited a slight decline. On the other hand, the t/l ratio was found to be increasing at 0.5 wt.% and 1 wt.% STF loadings but a substantial decrease was obtained in 3wt-STF/PU. The reason for the lower cell features of 3wt-STF/PU could be caused by agglomeration issues during the foaming process. Excessive STFs could be impaired cell nucleation and deteriorate the morphology of foam. This situation is frequently encountered during nanomaterial reinforcement [81, 83, 84]. Increased t/l ratio and cell density mean reduced localized stresses under the applied forces, leading to greater mechanical strength. In light of morphological characterizations and foam densities, 0.5wt-STF/PU and 1wt-STF/PU are possible candidates for higher compressive strength and energy absorption materials.

3.3 Compression tests of PU foams and their nanocomposites

PU foams and their nanocomposites are used as structural components for various applications. The definition of load-bearing capabilities of PU foams is important for structure safety. Due to the viscoelastic characteristics, PU foams exhibit strain rate dependent compressive response [39]. Compression tests were performed in order to understand load bearing capacity and rate dependent deformation behavior of neat PU foam and STF integrated PU foams.

The tests were carried out with using UTM, and the applied strain rates were 0.002, 0.02, and 0.2 s^{-1}. The compression test results, which are shown in Figure 3.6, distinctly represent the elastic, plateau, and densification regions, and compressive strengths and modulus are shared in Table 3.3 and Table 3.4 for all compositions, respectively. The results revealed that with the STF inclusion, the compressive strength of PU foams was found to be increased compared to neat, regardless of the strain rate. Similarly, in all three strain rates, the maximum compressive strength was exhibited by 1wt-STF/PU, beyond which the compressive strength deteriorated in 3wt-STF/PU. The highest increase in compressive strength was found to be 33% when the strain rate was 0.2 s^{-1}.

According to morphological characterizations, 1wt-STF26 was expected to demonstrate the highest compressive strength whereas the lowest for the neat because of their t/l ratio and cell densities. Compression test results are compatible with morphological investigations. The differences were distinguished clearly in the densification region with the collapsing and crushing of cells. This situation could be explained by the stiffness of cell walls. The maximum stress at the 80% strain increased more than 50% with 1 wt-STF26. Also, 3wt-STF26 demonstrated 15% higher maximum stress than neat PU foam.

Besides compressive strength, other crucial subjects are specific compressive strength for engineering applications. Specific compressive strength could be defined as strength per unit density. Especially for transportation vehicles, motorsports, civil, and military aviation, designers and engineers aim to reduce the total mass in order to improve performance [85, 86]. 10.4% enhancement was observed at specific

compression strength with 1wt-STF/PU at 0.2 s^{-1} strain rate. 8.4% and 6.1% increments were observed at 0.002 s^{-1} and 0.02 s^{-1}, respectively.

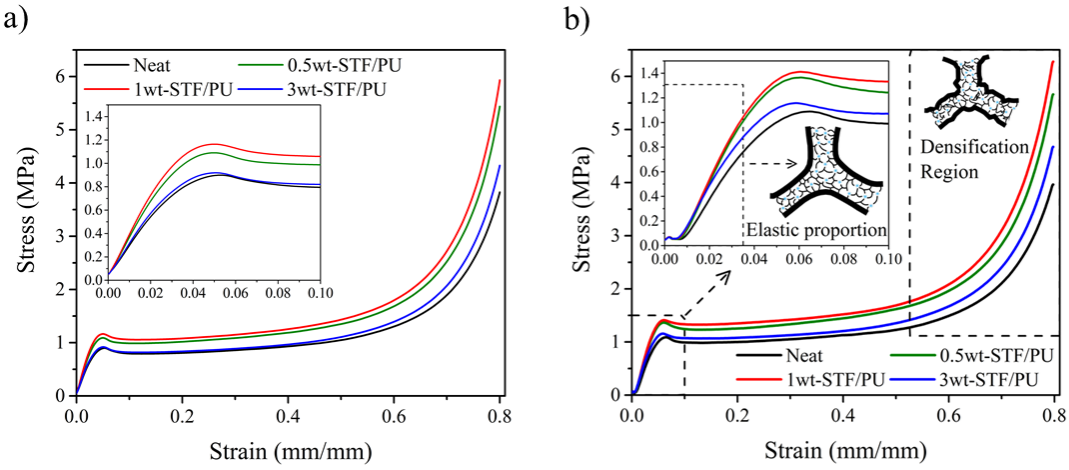

Figure 3.6: Compressive response of neat and STF/PU foams under different strain rates: a) 0.002 s^{-1}, b) 0.2 s^{-1}.

Table 3.3: Compressive response of neat and STF/PU foams.

Sample	Compressive Strength (MPa)			Enhancement at 0.002 s^{-1} / 0.02 s^{-1} / 0.2 s^{-1} (%)
	0.002 s^{-1}	0.02 s^{-1}	0.2 s^{-1}	
Neat	0.90 ±0.01	1.09 ±0.01	1.09 ±0.01	- / - / -
0.5wt-STF/PU	1.13 ±0.04	1.35 ±0.04	1.38 ±0.03	25.56 / 23.85 / 26.61
1wt-STF/PU	1.18 ±0.02	1.41 ±0.02	1.45 ±0.02	31.11 / 29.36 / 33.03
3wt-STF/PU	0.94 ±0.02	1.10 ±0.03	1.16 ±0.02	4.44 / 0.92 / 5.45

Table 3.4: Compressive modulus of neat and STF/PU foams.

Sample	Compressive Modulus (MPa)			Enhancement at 0.002 s^{-1} / 0.02 s^{-1} / 0.2 s^{-1} (%)
	0.002 s^{-1}	0.02 s^{-1}	0.2 s^{-1}	
Neat	24.04 ±0.69	28.82 ±0.87	28.92 ±0.71	- / - / -
0.5wt-STF/PU	32.09 ±1.99	37.25 ±1.17	38.57 ±0.58	33.50 / 29.25 / 33.35
1wt-STF/PU	35.83 ±0.88	40.02 ±0.68	39.97 ±1.67	49.07 / 38.87 / 38.22
3wt-STF/PU	26.57 ±0.77	30.24 ±0.53	30.87 ±0.23	10.53 / 4.94 / 6.82

Viscoelastic properties and shear thickening phenomena are time-dependent behavior of materials [87–89]. Time-dependent properties could be evaluated by considering the varying strain rate under applied loads [89–91]. Strain rate dependency of STF/PU and neat foam were investigated for this purpose. Compressive strengths and specific

compressive strength increased with increasing strain rates. However, compressive strength values of neat foam were equal for 0.02 $s^{-1}$and 0.2 s^{-1}. A major change in compressive strength was observed between 0.002 $s^{-1}$and 0.02 s^{-1}. On the other hand, at 0.2 s^{-1}compressive strength slightly increased for STF/PU foams. Energy absorption capabilities under cyclic loadings should be discussed for a deeper understanding of the effect of strain rate.

3.4 Cyclic compression tests of PU foams and their nanocomposites

Cyclic compression tests were carried out with UTM under different strain rates and strains for 10 cycles which were adequate for the short-term response of materials. The applied strains were 10%, 40%, and 80% in order to investigate energy absorption capabilities at elastic, plastic, and densification regions, respectively. ELC and loss factor values were obtained from loading-unloading curves. Cyclic compression tests of 1wt-STF/PU for 10% strain are demonstrated in Figure 3.7. Hysteresis area, loss factor, and ELC values decreased with the following cycles. A significant decrease in the second cycle was observed that could be explained by breaking van der Waals interactions and kink formations, disentanglement of PU chains, and deformation of cells [39, 92–94]. After the fifth cycle, stress-strain curves almost overlapped. ELC and loss factor values were calculated from the stress-strain diagrams for the 10th cycle for all conditions and compositions.

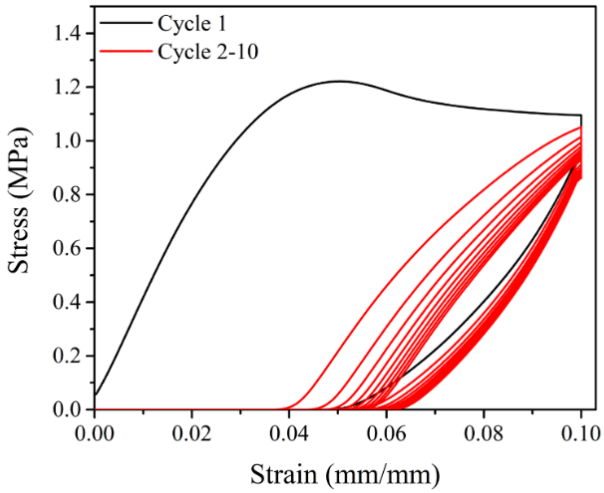

Figure 3.7: Cyclic compressive response of 1wt-STF/PU at 0.002 $s^{-1}$for 10% strain.

At the 10% strain, the hysteresis area of the foams increased with STF integration which is shown in Figure 3.8. 8.6% increment was obtained with 0.5wt-STF/PU and

1wt-STF/PU at 0.002 s^{-1}in loss factor as shown in Table 3.5. In addition, a 4.3% minor increase was observed with 3wt-STF/PU. However, the loss factor values almost 50% decreased with increasing strain rate for all compositions. 3wt-STF/PU demonstrated the lowest decrement with 44% when the strain rate increased. The loss factor increased with increasing STF content at 0.02 s^{-1}. 15.9% enhancement for the loss factor was obtained with 3wt-STF/PU.

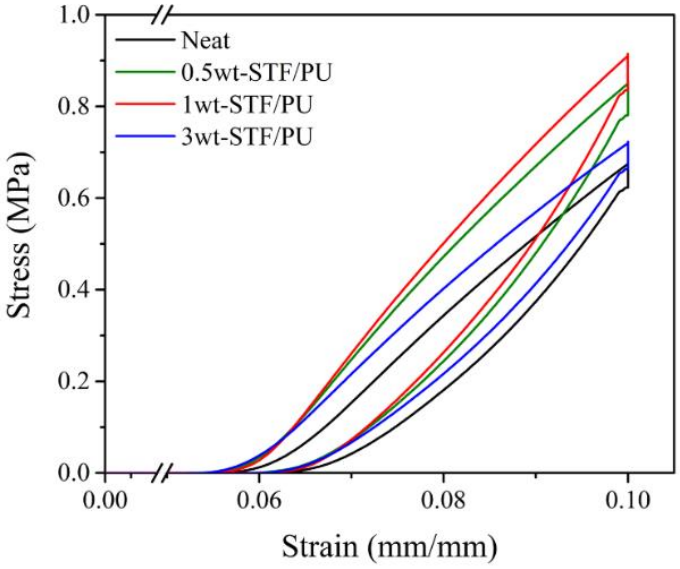

Figure 3.8: Cyclic compressive response of neat and STF/PU foams in the 10th cycle at 0.002 $s^{-1}$for 10% strain.

Table 3.5: Calculated loss factor and ELC values of neat, STF/PU foams in the 10th cycle and enhancement in loss factor at 0.02 $s^{-1}$for 10% strain.

10% Cyclic Compression	ELC (%)		Loss Factor		Enhancement at 0.02 s^{-1} (%)
	0.002 s^{-1}	0.02 s^{-1}	0.002 s^{-1}	0.02 s^{-1}	
Neat	34.5 ±0.2	19.1 ±0.5	0.133 ±0.001	0.067 ±0.002	-
0.5wt-STF/PU	37.0 ±0.5	20.0 ±0.4	0.144 ±0.003	0.07 ±0.002	6
1wt-STF/PU	36.9 ±0.5	20.7 ±0.2	0.144 ±0.002	0.073 ±0.01	9
3wt-STF/PU	35.6 ±0.4	21.8 ±0.4	0.139 ±0.002	0.078 ±0.003	16.4

The cyclic compression results of 1wt-STF/PU with different strain rates are demonstrated in Figure 3.9. 1wt-STF/PU absorbed lower energy with the increasing strain rate. In the 5 s holding section of 0.02 s^{-1} tests, the stress initially increased then stress softening was observed under constant strain after the second cycle. Similar trends were observed for all compositions. This situation could be explained by cell

and polymer chain movements. 0.002 s^{-1} and 0.2 s^{-1} strain rates were decided for the 40 and 80% strains in order to understand the capabilities of the samples.

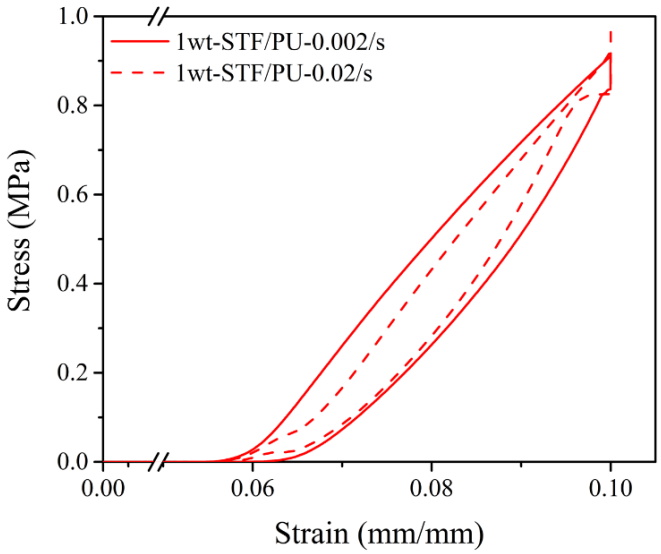

Figure 3.9: Cyclic compressive response of 1wt-STF/PU foam in the 10th cycle at 0.002 $s^{-1}$and 0.02 s^{-1}.

At the higher strains, ELC and loss factor values were merely affected by the STF integration for both strain rates. The obtained results are shared in Table 3.6 and Table 3.7. ELC and loss factor values increased with increasing strain rate, in contrast to the results at 10% strain. The difference could be explained by the change in the deformation of the cell walls and the viscoelastic nature of polymers. At lower strains, such as 10%, cell walls stretch under applied forces while the strain increases cell walls buckle and collapse.

As mentioned before, ELC and loss factor values are obtained from the hysteresis area, which equals to absorbed energy, and area under loading curves. The specific energy absorption can be quantitatively measured from the hysteresis area and divided by the density of the foam to determine the specific absorbed energy. ELC and loss factor values are unitless however specific absorbed energy could be measured as Joule per gram. Thus, energy absorption capabilities could be compared regardless of density. Specific absorbed energy and absorbed energy were calculated by summing up 10 cycles' hysteresis areas and demonstrated in Table 3.8 and Table 3.9. Absorbed energies dramatically increased with increasing applied strain due to the deformation of foam cells. ELC and loss factor values were not significantly changed by the STF integration for higher strains. However, increments in the energy absorption

capabilities with STF integration are clearly seen when the absorbed energy and specific absorbed energy values are taken into consideration. 1wt-STF/PU exhibited superior energy absorption properties up to 50% in absorbed energy and 22.3% in specific absorbed energy.

Table 3.6: Calculated loss factor and ELC values of neat and STF/PU foams in the 10^{th} cycle for 40% strain.

40% Cyclic Compression	ELC (%)		Loss Factor	
	0.002 s^{-1}	0.2 s^{-1}	0.002 s^{-1}	0.2 s^{-1}
Neat	50.6 ±0.2	63.1 ±0.2	0.216 ±0.001	0.293 ±0.001
0.5wt-STF/PU	50.9 ±0.5	62.9 ±0.1	0.217 ±0.003	0.292 ±0.001
1wt-STF/PU	50.9 ±0.3	61.8 ±0.3	0.217 ±0.002	0.285 ±0.002
3wt-STF/PU	52.0 ±0.2	63.8 ±0.2	0.224 ±0.001	0.298 ±0.002

Table 3.7: Calculated loss factor and ELC values of neat and STF/PU foams in the 10^{th} cycle for 80% strain.

80% Cyclic Compression	ELC (%)		Loss Factor	
	0.002 s^{-1}	0.2 s^{-1}	0.002 s^{-1}	0.2 s^{-1}
Neat	55.9 ±1.0	65.9 ±0.1	0.247 ±0.006	0.313 ±0.001
0.5wt-STF/PU	56.0 ±0.3	64.4 ±0.3	0.248 ±0.002	0.302 ±0.002
1wt-STF/PU	55.6 ±0.4	63.5 ±0.2	0.245 ±0.003	0.296 ±0.001
3wt-STF/PU	57.4 ±1.4	67.5 ±0.4	0.256 ±0.009	0.324 ±0.003

Table 3.8: Calculated absorbed energy values of neat and STF/PU foams.

Absorbed energy (MJ/m^3)*	10% strain		40% strain		80% strain	
	0.002 s^{-1}	0.02 s^{-1}	0.002 s^{-1}	0.2 s^{-1}	0.002 s^{-1}	0.2 s^{-1}
Neat	0.12	0.11	0.58	0.66	1.58	1.66
0.5wt-STF/PU	0.16	0.14	0.73	0.81	2.06	2.14
1wt-STF/PU	0.18	0.15	0.77	0.87	2.22	2.31
3wt-STF/PU	0.13	0.12	0.62	0.71	1.80	1.90

**STD values are lower than 0.01 for each sample and tests*

Absorbed energies dramatically increased with increasing applied strain due to the deformation of foam cells. ELC and loss factor values were not significantly changed

by the STF integration for higher strains. However, increments in the energy absorption capabilities with STF integration are clearly seen when the absorbed energy and specific absorbed energy values are taken into consideration. 1wt-STF/PU exhibited superior energy absorption properties up to 50% in absorbed energy and 22.3% in specific absorbed energy.

Table 3.9: Specific absorbed energy values of neat and STF/PU foams.

Specific absorbed energy (J/g)*	10% strain		40% strain		80% strain	
	0.002 s^{-1}	0.02 s^{-1}	0.002 s^{-1}	0.2 s^{-1}	0.002 s^{-1}	0.2 s^{-1}
Neat	1.26	1.19	6.10	6.98	16.65	17.48
0.5wt-STF/PU	1.42	1.27	6.40	7.09	18.12	18.85
1wt-STF/PU	1.54	1.34	6.70	7.63	19.41	20.21
3wt-STF/PU	1.30	1.19	5.99	6.93	17.51	18.52

**STD values are lower than 0.01 for each sample and tests*

3.5 Dynamic mechanical tests of neat and STF-Integrated PU foams

Dynamic mechanical tests of foams were investigated with dual cantilever geometry in order to obtain the material responses, under the different cyclic loads with sinusoidal waveform and the various frequencies which were classified as elastic and viscous behavior. Storage modulus corresponds to the elasticity of materials and loss modulus were energy dissipation such as heat or internal frictions [95, 96]. Actually, both of them aim to resistance to deformation in disparate ways. Strain-sweep tests were performed in order to understand linear viscoelastic region and test results are demonstrated in Figure 3.10. Linear viscoelastic region increased with STF integration. According to the engineering approach, materials are expected to remain in the elastic region during their service life, except in extreme cases such as impact and crash. By increasing the storage modulus and linear elastic region, STF/PU foams could withstand higher loads and strokes without permanent deformation.

Then frequency-sweep tests were performed in the linear viscoelastic region and the obtained results are demonstrated in Figure 3.11 and Table 3.10. Storage modulus and loss modulus increased with increasing STF content until 1 wt.%. The results were similar to the compression and cyclic compression test results although the applied force direction and frequency were different. Storage modulus and compression

modulus increased around 50% with 1 wt.% STF integration and no significant changes were observed in the loss factor.

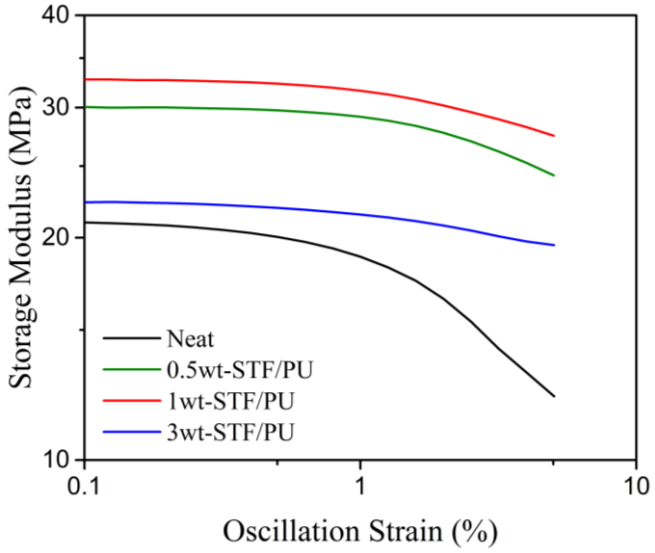

Figure 3.10: Strain-sweep tests of STF/PU foam.

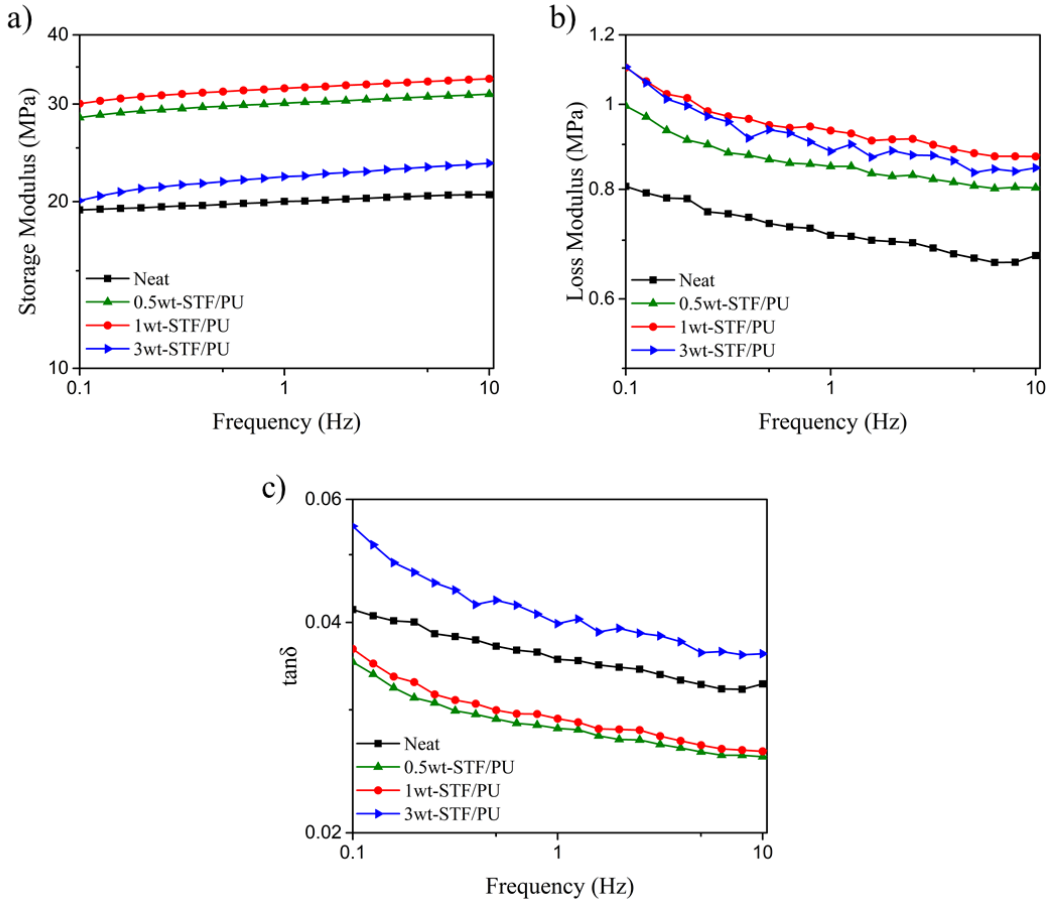

Figure 3.11: a) Storage modulus, b) loss modulus, and c) tanδ values of STF/PU foams under frequency-sweep tests.

Table 3.10: Storage modulus, loss modulus, and tanδ values of STF/PU foams under frequency-sweep tests at 1 Hz.

Sample	Storage Modulus (MPa)	Loss Modulus (MPa)	Loss factor tanδ	Enhancement in Storage / Loss Moduli (%)
Neat	20.96 ±1.91	0.73 ±0.05	0.035	- / -
0.5wt-STF/PU	30.28 ±0.49	0.84 ±0.03	0.028	44.5 / 15.1
1wt-STF/PU	32.39 ±3.83	0.98 ±0.03	0.031	54.5 / 34.3
3wt-STF/PU	24.95 ±3.19	0.88 ±0.02	0.036	19 / 20.1

4. CONCLUSION

The effect of STF integration into rigid PU foam was investigated under a wide strain range using different strain rates in order to understand the energy absorption and mechanical characteristics of STF/PU foams and their morphological structure. In this study, STF/PU foams demonstrated promising results for enhanced energy absorption and load bearing capacity of polymeric foam cores. Various weight fractions of silica and different silica geometries were investigated to optimize the STF composition where the maximum thickening behavior was observed with 26 wt.% fumed silica, after which lower performance associated with agglomerations occurred. Cellular structures of foams were affected by the STF integration where cell density and t/l ratio were found to be increasing with 0.5 and 1 wt.% STF integration whereas a slight decrease took place with 3 wt.% STF addition.

Accordingly, the changes in the morphological features altered the mechanical properties as well. The results revealed that strain rate has a positive effect on the compressive strength whereas up to 33% increase in compressive strength is viable with 1 wt.% STF addition. Additionally, 1 wt.% STF/PU foam demonstrated a 10.4% slight increase in the specific compression strength, tested at 0.2 s^{-1}. Furthermore, a significant 49.1% enhancement in compressive modulus was achieved when the strain rate was 0.002 s^{-1}.

Cyclic compression test results showed that ELC and loss factor values exhibited similar trends when evaluating the energy absorption capabilities of neat and STF/PU foams. ELC and loss factor increased with increasing applied strain as a result of the plastic deformation where cell walls buckle and absorb much higher energy. The energy absorption capabilities of PU foams increased substantially with increasing applied strain due to the deformation of the foam cells. While STFs had no noticeable effect on ELC and loss factor values at higher strains, improvements in energy absorption capabilities were evident when considering absorbed energy and specific absorbed energy values. Specifically, the addition of 1 wt.% STF integration resulted in superior energy absorption properties, with increases of up to 50% in absorbed

energy and 22.3% in specific absorbed energy for 10 cycle intervals. Dynamic mechanical analysis results showed that STF integration increases the linear viscoelastic region and 54.5% increment in storage modulus was observed with 1 wt.% STF/PU while the loss factor slightly decreased. The results of the study demonstrated that the addition of an optimized amount of STF could dramatically improve the compressive strength, viscoelastic properties, and energy absorption capabilities of PU foams. These strengthened mechanical properties broaden the possible applications of PU foams, allowing them to be used in a wider range of conditions and to build safer and more reliable engineering structures.

In consideration of the sustainable impact of this study, the enhancement of specific compressive stress, and specific absorbed energy in materials plays a prominent role in improving their structural performance. This improvement enables the materials to withstand higher loads and absorb the applied energy with lightweight. The findings of the study revealed that the integration of a 1 wt.% STF into PU foam yielded the most favorable outcomes, demonstrating a notable increment in specific compressive stress and specific absorbed energy. However, it is worth noting that acceptable results were still achieved with a 0.5 wt.% STF integration. Consequently, in applications where factors such as sustainability, cost-effectiveness, and time efficiency hold significant importance, the utilization of the 0.5 wt.% STF integrated PU foam could be preferred.

REFERENCES

[1] **Sun, L., Gibson, R. F., Gordaninejad, F., & Suhr, J.** (2009). Energy absorption capability of nanocomposites: A review. *Composites Science and Technology*, *69*(14), 2392–2409. https://doi.org/10.1016/j.compscitech.2009.06.020

[2] **Akindoyo, J. O., Beg, M. D. H., Ghazali, S., Islam, M. R., Jeyaratnam, N., & Yuvaraj, A. R.** (2016). Polyurethane types, synthesis and applications-a review. *RSC Advances*, *6*(115), 114453–114482. https://doi.org/10.1039/c6ra14525f

[3] **Tarlochan, F., Ramesh, S., & Harpreet, S.** (2012). Advanced composite sandwich structure design for energy absorption applications: Blast protection and crashworthiness. *Composites Part B: Engineering*, *43*(5), 2198–2208. https://doi.org/10.1016/j.compositesb.2012.02.025

[4] **Gunton P., Nickels L.** (2014). Reinforced Plastics. In Gunton P., Nickels L. (Eds.), *Foam Core Impresses in Aircraft Study* (Vol. 58, Issue 6 pp. 31–33). London: Elsevier. https://doi.org/10.1016/S0034-3617(14)70248-6.

[5] **Khan, T., Acar, V., Aydin, M. R., Hülagü, B., Akbulut, H., & Seydibeyoğlu, M. Ö.** (2020). A review on recent advances in sandwich structures based on polyurethane foam cores. *Polymer Composites*, *41*(6), 2355–2400. https://doi.org/10.1002/pc.25543

[6] **Ribeiro Da Silva, V., Mosiewicki, M. A., Yoshida, M. I., Coelho Da Silva, M., Stefani, P. M., & Marcovich, N. E.** (2013). Polyurethane foams based on modified tung oil and reinforced with rice husk ash I: Synthesis and physical chemical characterization. *Polymer Testing*, *32*(2), 438–445. https://doi.org/10.1016/j.polymertesting.2013.01.002

[7] **Vaithylingam, R., Ansari, M. N. M., & Shanks, R. A.** (2017). Recent Advances in Polyurethane-Based Nanocomposites: A Review. *Polymer - Plastics Technology and Engineering*, *56*(14), 1528–1541. https://doi.org/10.1080/03602559.2017.1280683

[8] **Gupta, R. K., & Kahol, P. K.** (2021). Polyurethane Chemistry: Renewable Polyols and Isocyanates. In F. M. De Souza, R. K. Gupta, P. K. Kahol (Eds)**.** *Introduction to Polyurethane Chemistry* (1st ed., Vol. 1380, pp. 1-24) . Washington, DC : American Chemical Soceity.

[9] **Ashida, K.** (2007). *P*olyurethane and related foams: Chemistry and technology. In, K. Ashida (Eds.), *Polyurethane Foams* (1st ed. Vol. 1, pp.65-96). Boca Raton, FL: CRC Press.

[10] **Santiago-Calvo, M., Tirado-Mediavilla, J., Ruiz-Herrero, J. L., Rodríguez-Pérez, M. Á., & Villafañe, F.** (2018). The effects of functional nanofillers on the reaction kinetics, microstructure, thermal and mechanical properties of water blown rigid polyurethane foams. *Polymer*, *150*, 138–149. https://doi.org/10.1016/j.polymer.2018.07.029

[11] **Gama, N. V., Ferreira, A., & Barros-Timmons, A.** (2018). Polyurethane foams: Past, present, and future. *Materials*, *11*(10), 1-35. https://doi.org/10.3390/ma11101841

[12] **Lee, S. T.** (2016). Polymeric foams: Innovations in processes, technologies, and products. In W. Ma, K. Feichtinger (Eds.), *Rigid Structural Foam and Foam-Cored Sandwich Composites* (1st ed. Vol. 1, pp. 257-316). Boca Raton, FL: CRC Press.

[13] **Burgaz, E.** (2019). *Polyurethane Insulation Foams for Energy and Sustainability.* Cham, Springer Nature Switzerland AG.

[14] **Cimavilla-Román, P., Santiago-Calvo, M., & Rodríguez-Pérez, M. Á.** (2021). Dynamic Mechanical Analysis during polyurethane foaming: Relationship between modulus build-up and reaction kinetics. *Polymer Testing*, *103*, 1-10. https://doi.org/10.1016/j.polymertesting.2021.107336

[15] **Choe, K. H., Soo, D. L., Seo, W. J., & Kim, W. N.** (2004). Properties of rigid polyurethane foams with blowing agents and catalysts. *Polymer Journal*, *36*(5), 368–373. https://doi.org/10.1295/polymj.36.368

[16] **Espadas-Escalante, J. J., & Avilés, F.** (2015). Anisotropic compressive properties of multiwall carbon nanotube/polyurethane foams. *Mechanics of Materials*, *91*(P1), 167–176. https://doi.org/10.1016/j.mechmat.2015.07.006

[17] **Pikhurov, D. V., Sakhatskii, A. S., & Zuev, V. V.** (2018). Rigid polyurethane foams with infused hydrophilic/hydrophobic nanoparticles: Relationship between cellular structure and physical properties. *European Polymer Journal*, *99*, 403–414. https://doi.org/10.1016/j.eurpolymj.2017.12.036

[18] **Caglayan, C., Gurkan, I., Gungor, S., & Cebeci, H.** (2018). The effect of CNT-reinforced polyurethane foam cores to flexural properties of sandwich composites. *Composites Part A: Applied Science and Manufacturing*, *115*, 187–195. https://doi.org/10.1016/j.compositesa.2018.09.019

[19] **Hawkins, M. C., O'Toole, B., & Jackovich, D.** (2005). Cell morphology and mechanical properties of rigid polyurethane foam. *Journal of Cellular Plastics*, *41*(3), 267–285. https://doi.org/10.1177/0021955X05053525

[20] **Ahn, W. S., & Lee, J. M.** (2015). Effect of CNT as a nucleating agent on cell morphology and thermal insulation property of the rigid polyurethane foams. *Journal of Nanoscience and Nanotechnology*, *15*(11), 9125–9130. https://doi.org/10.1166/jnn.2015.11564

[21] **Bernal, M. M., Lopez-Manchado, M. A., & Verdejo, R.** (2011). In situ foaming evolution of flexible polyurethane foam nanocomposites. *Macromolecular Chemistry and Physics*, *212*(9), 971–979. https://doi.org/10.1002/macp.201000748

[22] **Sung, G., Choe, H., Choi, Y., & Kim, J. H.** (2018). Morphological, acoustical, and physical properties of free-rising polyurethane foams depending on the flow directions. *Korean Journal of Chemical Engineering*, *35*(4), 1045–1052. https://doi.org/10.1007/s11814-017-0328-2

[23] **Chen, Y., Das, R., & Battley, M.** (2017). Effects of cell size and cell wall thickness variations on the strength of closed-cell foams. *International Journal of Engineering Science*, *120*, 220–240. https://doi.org/10.1016/j.ijengsci.2017.08.006

[24] **Bernal, M. M., Martin-Gallego, M., Molenberg, I., Huynen, I., López Manchado, M. A., & Verdejo, R.** (2014). Influence of carbon nanoparticles on the polymerization and EMI shielding properties of PU nanocomposite foams. *RSC Advances*, *4*(16), 7911–7918.

https://doi.org/10.1039/c3ra45607b

[25] **Valipour, F., Dehghan, S. F., & Hajizadeh, R.** (2022). The effect of nano- and microfillers on thermal properties of Polyurethane foam. *International Journal of Environmental Science and Technology*, *19*(1), 541–552. https://doi.org/10.1007/s13762-021-03150-3

[26] **Wang, S., Huang, X., & Zhang, W.** (2021). Preparation of graphene/flaky carbonyl iron/polyurethane foam composites and research on their microwave absorption properties. *Applied Physics A: Materials Science and Processing*, *127*(10), 1–11. https://doi.org/10.1007/s00339-021-04894-y

[27] **Chen, L., Rende, D., Schadler, L. S., & Ozisik, R.** (2013). Polymer nanocomposite foams. *Journal of Materials Chemistry A*, *1*(12), 3837–3850. https://doi.org/10.1039/c2ta00086e

[28] **Lorusso, C., Vergaro, V., Conciauro, F., Ciccarella, G., & Congedo, P. M.** (2017). Thermal and mechanical performance of rigid polyurethane foam added with commercial nanoparticles. *Nanomaterials and Nanotechnology*, *7*, 1–9. https://doi.org/10.1177/1847980416684117

[29] **Liu, Shanqiu, Eijkelenkamp, R., Duvigneau, J., & Vancso, G. J.** (2017). Silica-Assisted Nucleation of Polymer Foam Cells with Nanoscopic Dimensions: Impact of Particle Size, Line Tension, and Surface Functionality. *ACS Applied Materials and Interfaces*, *9*(43), 37929–37940. https://doi.org/10.1021/acsami.7b11248

[30] **Yan, D., Xu, L., Chen, C., Tang, J., Ji, X., & Li, Z.** (2012). Enhanced mechanical and thermal properties of rigid polyurethane foam composites containing graphene nanosheets and carbon nanotubes. *Polymer International*, *61*(7), 1107–1114. https://doi.org/10.1002/pi.4188

[31] **Saha, M. C., Kabir, M. E., & Jeelani, S.** (2008). Enhancement in thermal and mechanical properties of polyurethane foam infused with nanoparticles. *Materials Science and Engineering A*, *479*(1–2), 213–222. https://doi.org/10.1016/j.msea.2007.06.060

[32] **Mahfuz, H., Rangari, V. K., Islam, M. S., & Jeelani, S.** (2004). Fabrication, synthesis and mechanical characterization of nanoparticles infused polyurethane foams. *Composites Part A: Applied Science and Manufacturing*, *35*(4), 453–460. https://doi.org/10.1016/j.compositesa.2003.10.009

[33] **Xu, Z., Tang, X., Gu, A., & Fang, Z.** (2007). Novel preparation and mechanical properties of rigid polyurethane foam/organoclay nanocomposites. *Journal of applied polymer science*, 106(1), 439-447. (n.d.). https://doi.org/10.1002/app

[34] **Linul, E., Şerban, D. A., Marsavina, L., & Sadowski, T.** (2017). Assessment of collapse diagrams of rigid polyurethane foams under dynamic loading conditions. *Archives of Civil and Mechanical Engineering*, *17*(3), 457–466. https://doi.org/10.1016/j.acme.2016.12.009

[35] **Belingardi, G., Montanini, R., & Avalle, M.** (2001). Characterization of polymeric structural foams under compressive impact loading by means of energy-absorption diagram. *International Journal of Impact Engineering*, *25*(5), 455–472.

[36] **Ouellet, S., Cronin, D., & Worswick, M.** (2006). Compressive response of polymeric foams under quasi-static, medium and high strain rate

conditions. *Polymer Testing*, *25*(6), 731–743. https://doi.org/10.1016/j.polymertesting.2006.05.005

[37] **Daphalapurkar, N. P., Hanan, J. C., Phelps, N. B., Bale, H., & Lu, H.** (2008). Tomography and simulation of microstructure evolution of a closed-cell polymer foam in compression. *Mechanics of Advanced Materials and Structures*, *15*(8), 594–611. https://doi.org/10.1080/15376490802470523

[38] **Ashby, M. F.** (1983). Mechanical Properties of Cellular Solids. *Metallurgical Transactions. A, Physical Metallurgy and Materials Science*, *14 A*(9), 1755–1769. https://doi.org/10.1007/BF02645546

[39] **Bhinder, J., & Agnihotri, P. K.** (2020). Effect of carbon nanotube doping on the energy dissipation and rate dependent deformation behavior of polyurethane foams. *Journal of Cellular Plastics, 57*(3):287-311. https://doi.org/10.1177/0021955X20917280

[40] **Cura', F., Sesana, R., Zhang, X. C., Scarpa, F., Lu, W. J., & Peng, H. X.** (2019). Stiffness, Energy Dissipation, and Hyperelasticity in Hierarchical Multilayer Composite Nanocoated Open-Cell Polyurethane Foams. *Advanced Engineering Materials*, *21*(12), 1–12. https://doi.org/10.1002/adem.201900459

[41] **Lu, W., Qin, F., Zhang, Q., Remillat, C., Wang, H., Scarpa, F., & Peng, H. X.** (2020). Engineering foam skeletons with multilayered graphene oxide coatings for enhanced energy dissipation. *Composites Part A: Applied Science and Manufacturing*, *137*, 106035. https://doi.org/10.1016/j.compositesa.2020.106035

[42] **Wang, Y., Lu, J., Zhai, X., Xue, B., & Zhi, X.** (2019). Response of energy absorbing connector with polyurethane foam and multiple pleated plates under impact loading. *International Journal of Impact Engineering*, *13*, 103356. https://doi.org/10.1016/j.ijimpeng.2019.103356

[43] **Schmitz, T. L., & Smith, K. S.** (2012). Mechanical vibrations: Modeling and measurement. In T. L. Schmitz, K. S. Smith (Eds), *Vibration Control* (5th ed., Vol. 1, pp. 769-869). Upper Saddle River, NJ: Pearson Education, Inc.

[44] **Wagner, M.** (2018). Thermal Analysis in Practice: Fundamental Aspects. In H. W. Starkweather (Eds.), *Dynamic Mechanical Analysis* (1st ed.,Vol. 1, pp. 210-240). Munich: Hanser.

[45] **Van Krevelen, D. W., & Te Nijenhuis, K.** (2009). Properties of Polymers:Their Correlation With Chemical Structure; Their Numerical Estimation and Prediction From Additive Group Contributions. In birileri (Eds.), *Mechanical Properties of Solid Polymers* (4th ed., Vol. 1, pp. 383-500). Amsterdam: Elsevier.

[46] **Liu, Shaobo, Li, A., He, S., & Xuan, P.** (2015). Cyclic compression behavior and energy dissipation of aluminum foam-polyurethane interpenetrating phase composites. *Composites Part A: Applied Science and Manufacturing*, *78*, 35–41. https://doi.org/10.1016/j.compositesa.2015.07.016

[47] **Bhinder, J., & Agnihotri, P. K.** (2019). Synthesis and characterization of poly-urethane foam doped with different nano-fillers. *Materials Today: Proceedings*, *18*, 1479–1488. https://doi.org/10.1016/j.matpr.2019.06.617

[48] **Xu, Z., Wang, G., Zhao, J., Zhang, A., & Zhao, G.** (2022). Super-elastic and structure-tunable poly(ether-block-amide) foams achieved by microcellular foaming. *Journal of CO2 Utilization*, *55*, 101807. https://doi.org/10.1016/j.jcou.2021.101807

[49] **Darvizeh, A., Darvizeh, M., Ansari, R., & Meshkinzar, A.** (2013). Effect of low density, low strength polyurethane foam on the energy absorption characteristics of circumferentially grooved thick-walled circular tubes. *Thin-Walled Structures*, *71*, 81–90. https://doi.org/10.1016/j.tws.2013.04.014

[50] **Oh, J. H., Kim, J. S., Nguyen, V. H., & Oh, I. K.** (2020). Auxetic graphene oxide-porous foam for acoustic wave and shock energy dissipation. *Composites Part B: Engineering*, *186*, 107817. https://doi.org/10.1016/j.compositesb.2020.107817

[51] **Adnan, S. A., Samsudin, S. N., Zainuddin, F., Azizan, N. A., Akil, H. M., & Ahmad, S.** (2014). Effect of carbon nanotubes on the compression test and energy absorption of aluminium/polyurethane-carbon nanotubes foam sandwich. *Key Engineering Materials*, *594–595*, 686–690. https://doi.org/10.4028/www.scientific.net/KEM.594-595.686

[52] **Navidfar, A., Sancak, A., Yildirim, K. B., & Trabzon, L.** (2018). A Study on Polyurethane Hybrid Nanocomposite Foams Reinforced with Multiwalled Carbon Nanotubes and Silica Nanoparticles. *Polymer - Plastics Technology and Engineering*, *57*(14), 1463–1473. https://doi.org/10.1080/03602559.2017.1410834

[53] **Yang, C., Chen, Z., Yao, S., Xu, P., Li, S., & Alqahtani, M. S.** (2022). Parametric study on the crushing performance of a polyurethane foam-filled CFRP/Al composite sandwich structure. *Polymer Testing*, *108*, 107515. https://doi.org/10.1016/j.polymertesting.2022.107515

[54] **Sun, Y., & Li, Q. M.** (2015). Effect of entrapped gas on the dynamic compressive behaviour of cellular solids. *International Journal of Solids and Structures*, *63*, 50–67. https://doi.org/10.1016/j.ijsolstr.2015.02.034

[55] **Sadot, O., Ram, O., Anteby, I., Gruntman, S., & Ben-Dor, G.** (2016). The trapped gas effect on the dynamic compressive strength of light aluminum foams. *Materials Science and Engineering A*, *659*, 278–286. https://doi.org/10.1016/j.msea.2016.02.031

[56] **Fu, K., Wang, H., Zhang, Y. X., Ye, L., Escobedo, J. P., Hazell, P. J., Friedrich, K., & Dai, S.** (2020). Rheological and energy absorption characteristics of a concentrated shear thickening fluid at various temperatures. *International Journal of Impact Engineering*, *139*, 103525. https://doi.org/10.1016/j.ijimpeng.2020.103525

[57] **Caglayan, C., Gurkan, I., Gungor, S., & Cebeci, H.** (2018). The effect of CNT-reinforced polyurethane foam cores to flexural properties of sandwich composites. *Composites Part A: Applied Science and Manufacturing*, *115*, 187–195. https://doi.org/10.1016/j.compositesa.2018.09.019

[58] **Soutrenon, M., & Michaud, V.** (2014). Impact properties of shear thickening fluid impregnated foams. *Smart Materials and Structures*, *23*(3), 1-10. https://doi.org/10.1088/0964-1726/23/3/035022

[59] **Haris, A., Goh, B. W. Y., Tay, T. E., Lee, H. P., Rammohan, A. V, & Tan, V. B. C.** (2018). On the effectiveness of incorporating shear thickening fluid with fumed silica particles in hip protectors. *Smart Materials and Structures*, *27*(1), 015021. https://doi.org/10.1088/1361-665X/aa9e60

[60] **Gürgen, S., Kuşhan, M. C., & Li, W.** (2017). Shear thickening fluids in protective applications: A review. *Progress in Polymer Science*, *75*, 48–72. https://doi.org/10.1016/j.progpolymsci.2017.07.003

[61] **Hoffman, R. L.** (1972). Discontinuous and dilatant viscosity behavior in concentrated suspensions. I. Observation of a flow instability. *Transactions of the Society of Rheology*, *16*, 155–173. https://doi.org/10.1122/1.549250

[62] **Bossis, G., Brady, J. F.** (1989). The rheology of Brownian suspensions. *The Journal of Chemical Physics*, *91*(3), 1866–1874. https://doi.org/10.1063/1.457091

[63] **Brown, E., Jaeger, H. M.** (2012). The role of dilation and confining stresses in shear thickening of dense suspensions. *Journal of Rheology*, *56*, 4709423. https://doi.org/10.1122/1.4709423.

[64].**Wei, M., Lin, K., & Sun, L.** (2022). Shear thickening fluids and their applications. *Materials and Design*, *216*, 110570. https://doi.org/10.1016/j.matdes.2022.110570

[65] **Yu, M., Qiao, X., Dong, X., & Sun, K.** (2018). Shear thickening effect of the suspensions of silica nanoparticles in PEG with different particle size, concentration, and shear. *Colloid and Polymer Science*, *296*(7), 1119–1126. https://doi.org/10.1007/s00396-018-4325-8

[66].**Bajya, M., Majumdar, A., Butola, B. S., Verma, S. K., & Bhattacharjee, D.** (2020). Design strategy for optimising weight and ballistic performance of soft body armour reinforced with shear thickening fluid. *Composites Part B: Engineering*, *183*, 107721. https://doi.org/10.1016/j.compositesb.2019.107721

[67] **Decker, M. J., Halbach, C. J., Nam, C. H., Wagner, N. J., & Wetzel, E. D.** (2007). Stab resistance of shear thickening fluid (STF)-treated fabrics. *Composites Science and Technology*, *67*(3–4), 565–578. https://doi.org/10.1016/j.compscitech.2006.08.007

[68] **Warren, J., Cole, M., Offenberger, S., Kota, K. R., Lacy, T. E., Toghiani, H., Burchell, M., Kundu, S., & Pittman, C. U.** (2021). Hypervelocity Impacts on Honeycomb Core Sandwich Panels Filled with Shear Thickening Fluid. *International Journal of Impact Engineering*, *150*, 103803. https://doi.org/10.1016/j.ijimpeng.2020.103803

[69] **Zhu, J. Q., Gu, Z. P., Liu, Z. P., Zhong, F. C., Wu, X. Q., & Huang, C. G.** (2022). Silicone rubber matrix composites with shear thickening fluid microcapsules realizing intelligent adaptation to impact loadings. *Composites Part B: Engineering*, *247*, 110312. https://doi.org/10.1016/j.compositesb.2022.110312

[70] **Hu, Q., Lu, G., Hameed, N., & Tse, K. M.** (2022). Dynamic compressive behaviour of shear thickening fluid-filled honeycomb. *International Journal of Mechanical Sciences*, *229*, 107493. https://doi.org/10.1016/j.ijmecsci.2022.107493

[71] **Wu, Y., Wang, S., Sang, M., Shu, Q., Zhang, J., Xuan, S., & Gong, X.** (2021). A safeguarding and high temperature tolerant organogel electrolyte for flexible solid-state supercapacitors. *Journal of Power Sources*, *505*, 230083. https://doi.org/10.1016/j.jpowsour.2021.230083

[72] **Pinto, F., & Meo, M.** (2017). Design and Manufacturing of a Novel Shear Thickening Fluid Composite (STFC) with Enhanced out-of-Plane Properties and Damage Suppression. *Applied Composite Materials*,

24(3), 643–660. https://doi.org/10.1007/s10443-016-9532-1

[73] **Liu, M., Zhang, S., Liu, S., Cao, S., Wang, S., Bai, L., Sang, M., Xuan, S., Jiang, W., & Gong, X.** (2019). CNT/STF/Kevlar-based wearable electronic textile with excellent anti-impact and sensing performance. *Composites Part A: Applied Science and Manufacturing*, *126*, 105612. https://doi.org/10.1016/j.compositesa.2019.105612

[74] **Cao, X., James Lee, L., Widya, T., & Macosko, C.** (2005). Polyurethane/clay nanocomposites foams: Processing, structure and properties. *Polymer*, *46*(3), 775–783. https://doi.org/10.1016/j.polymer.2004.11.028

[75] **Zhang, C., Hu, J., Chen, S., & Ji, F.** (2010). Theoretical study of hydrogen bonding interactions on MDI-based polyurethane. *Journal of Molecular Modeling*, *16*(8), 1391–1399. https://doi.org/10.1007/s00894-010-0645-4

[76] **Tien, Y. I., & Wei, K. H.** (2001). Hydrogen bonding and mechanical properties in segmented montmorillonite/polyurethane nanocomposites of different hard segment ratios. *Polymer*, *42*(7), 3213–3221. https://doi.org/10.1016/S0032-3861(00)00729-1

[77] **Bistričić, L., Baranović, G., Leskovac, M., & Bajsić, E. G.** (2010). Hydrogen bonding and mechanical properties of thin films of polyether-based polyurethane-silica nanocomposites. *European Polymer Journal*, *46*(10), 1975–1987. https://doi.org/10.1016/j.eurpolymj.2010.08.001

[78] **Fei, Y., Chen, F., Fang, W., Xu, L., Ruan, S., Liu, X., Zhong, M., & Kuang, T.** (2020). High-strength, flexible and cycling-stable piezo-resistive polymeric foams derived from thermoplastic polyurethane and multi-wall carbon nanotubes. *Composites Part B: Engineering*, *199*, 108279. https://doi.org/10.1016/j.compositesb.2020.108279

[79] **Żurowski, R., Falkowski, P., Zygmuntowicz, J., & Szafran, M.** (2021). Rheological and technological aspects in designing the properties of shear thickening fluids. *Materials*, *14*(21), 1-25. https://doi.org/10.3390/ma14216585

[80] **Chu, P., Zhang, H., Chen, F., & Zhang, Z.** (2016). Rheological behaviors of nanosilica suspensions with different dispersion levels prepared by the bead milling technique. *Composites Part A: Applied Science and Manufacturing*, *81*, 34–40. https://doi.org/10.1016/j.compositesa.2015.10.018

[81] **Pardo-Alonso, S., Solórzano, E., & Rodriguez-Perez, M. A.** (2013). Time-resolved X-ray imaging of nanofiller-polyurethane reactive foam systems. *Colloids and Surfaces A: Physicochemical and Engineering Aspects*, *438*, 119–125. https://doi.org/10.1016/j.colsurfa.2013.01.045

[82] **Merillas, B., Villafañe, F., & Rodríguez-Pérez, M. Á.** (2021). Nanoparticles addition in pu foams: The dramatic effect of trapped-air on nucleation. *Polymers*, *13*(17), 1–11. https://doi.org/10.3390/polym13172952

[83] **Kabir, M. E., Saha, M. C., & Jeelani, S.** (2007). Effect of ultrasound sonication in carbon nanofibers/polyurethane foam composite. *Materials Science and Engineering A*, *459*(1–2), 111–116. https://doi.org/10.1016/j.msea.2007.01.031

[84] **Nik Pauzi, N. N. P., A. Majid, R., Dzulkifli, M. H., & Yahya, M. Y.** (2014). Development of rigid bio-based polyurethane foam reinforced with nanoclay. *Composites Part B: Engineering*, *67*, 521–526. https://doi.org/10.1016/j.compositesb.2014.08.004

[85] **Holmes, M.** (2017). Aerospace looks to composites for solutions. *Reinforced Plastics*, *61*(4), 237–241. https://doi.org/10.1016/j.repl.2017.06.079

[86] **Kobayashi, S., Plotkin, S., & Ribeiro, S. K.** (2009). Energy efficiency technologies for road vehicles. *Energy Efficiency*, *2*(2), 125–137. https://doi.org/10.1007/s12053-008-9037-3

[87] **Kim, J. S., Arronche, L., Farrugia, A., Muliana, A., & La Saponara, V.** (2011). Multi-scale modeling of time-dependent response of smart sandwich constructions. *Composite Structures*, *93*(9), 2196–2207. https://doi.org/10.1016/j.compstruct.2011.03.006

[88] **Apostol, D. A., & Constantinescu, D. M.** (2013). Temperature and speed of testing influence on the densification and recovery of polyurethane foams. *Mechanics of Time-Dependent Materials*, *17*(1), 111–136. https://doi.org/10.1007/s11043-012-9179-8

[89] **Zhao, Q., Yuan, J., Jiang, H., Yao, H., & Wen, B.** (2021). Vibration control of a rotor system by shear thickening fluid dampers. *Journal of Sound and Vibration*, *494*, 115883. https://doi.org/10.1016/j.jsv.2020.115883

[90] **Poapongsakorn, P., & Kanchanomai, C.** (2011). Time-dependent deformation of closed-cell PVC foam. *Journal of Cellular Plastics*, *47*(4), 323–336. https://doi.org/10.1177/0021955X11401014

[91] **Basit, M. M., & Cheon, S. S.** (2019). Time-dependent crashworthiness of polyurethane foam. *Mechanics of Time-Dependent Materials*, *23*(2), 207–221. https://doi.org/10.1007/s11043-018-9391-2

[92] **Suhr, J., Victor, P., Ci, L., Sreekala, S., Zhang, X., Nalamasu, O., & Ajayan, P. M.** (2007). Fatigue resistance of aligned carbon nanotube arrays under cyclic compression. *Nature Nanotechnology*, *2*(7), 417–421. https://doi.org/10.1038/nnano.2007.186

[93] **Nautiyal, P., Boesl, B., & Agarwal, A.** (2018). The mechanics of energy dissipation in a three-dimensional graphene foam with macroporous architecture. *Carbon*, *132*, 59–64. https://doi.org/10.1016/j.carbon.2018.02.028

[94] **Kaushiva, B. D., Dounis, D. V., & Wilkes, G. L.** (2000). Influences of copolymer polyol on structural and viscoelastic properties in molded flexible polyurethane foams. *Journal of Applied Polymer Science*, *78*(4), 766–786. https://doi.org/10.1002/1097-4628(20001024)78:4<766::AID-APP100>3.0.CO;2-G

[95] **Kopal, I., Harničárová, M., Valíček, J., & Kušnerová, M.** (2017). Modeling the temperature dependence of dynamic mechanical properties and visco-elastic behavior of thermoplastic polyurethane using artificial neural network. *Polymers*, *9*(10), 1-17. https://doi.org/10.3390/polym9100519

[96] **Wieleba, W.** (2005). The role of internal friction in the process of energy dissipation during PTFE composite sliding against steel. *Wear*, *258*(5–6), 870–876. https://doi.org/10.1016/j.wear.2004.09.076

CURRICULUM VITAE

Name Surname : Emre GÜNDÜZ

EDUCATION

- B.Sc.: 2019, Gebze Technical University, Faculty of Engineering, Material Science and Engineering
- M.Sc : 2023, Istanbul Technical University, Graduate, School, Polymer Science and Technology

PROFESSIONAL EXPERIENCE AND REWARDS:

- 2021-2023 TUBITAK 3501 Project - Researcher Investigation of Viscoelastic Material Use for Enhancement of Vibrational Properties of Tensegrity Structures for Space Applications
- 2022 TUBITAK 2224-A Grant Program for Participation in Scientific Meetings Abroad for 2022 Material Research Socitey (MRS) FALL Meeting and Exhibit in Boston, MA, USA.

PUBLICATIONS, PRESENTATIONS AND PATENTS ON THE THESIS

- Gunduz Emre, Karagoz Bunyamin, Osken Ipek, Yildiz Kaan, Cebeci Hulya. 2022: Energy Dissipation and Rate-Dependent Deformation Behavior of STF-Integrated PU Foam Nanocomposites. International Congress - Material Research Socitey (MRS) FALL Meeting and Exhibit, November 27 - December 2, 2022 Boston, MA, USA.